Alma Mater Studiorum - Università di Bologna

School of Science
Department of Physics and Astronomy
Master Degree Programme in Astrophysics and Cosmology

Gravitational wave background and observed galaxy merger rate

Graduation Thesis

Presented by:
Nicolò Cedola

Supervisor:
Chiar.mo Prof. Carlo Nipoti

Academic year 2024-2025
Graduation date V

Si in terrarum orbem fuisse paulum bonitatem,
Et unusquisque fratrem suum considerasse
Ibi esset minus cogitationes minusque dolores
Et mundus esset consequuntur quanto magis pulcher.

Anonimo

Abstract

The NANOGrav and others Pulsar Timing Arrays (PTAs) have released data confirming the presence of a Stochastic Gravitational Wave Background (SGWB) in the nHz frequency range. The current understanding of its origin is that it is generated by astrophysical sources, i.e. the mergers of Super Massive Black Holes (SMBHs) following their host's merger, but there is still the possibility that this signal was generated in the early Universe from so-called cosmological sources. The objective of this work is focused on the astrophysical sources case, in particular it is an analysis of the SGWB using observed galactic merger rates to get information on the mechanisms of the SMBHs approach inside the newly formed galaxies. To achive this goal, a mock SGWB was built based on the observed galactic merger rates with a few parameters describing the unknown mechanisms of SMBH approach, searching for the values that maximised the likelihood of the models. The results seems to favour both prospects, meaning that the SGWB has both an astrophysical component and a cosmological component. The possibility of a singular strong source in one of the bin is also discussed, giving a criterion for the individuation of its host galaxy.

Sommario

NANOGrav e altre Pulsar Timing Arrays (PTAs) hanno rilasciato dei dati che confermano la presenza di uno Stochastic Gravitational Wave Background (SGWB) nel range di frequenze dei nHz. Attualmente si ritiene che la sua origine sia legata a sorgenti astrofisiche, i.e. la fusione di Super Massive Black Holes (SMBHs) conseguenti alla fusione di galassie, ma c'è ancora la possibilità che questo segnale sia invece stato generato nell'Universo primordiale da parte di cosiddette sorgenti cosmologiche. L'obbiettivo di questa tesi si focalizza sul caso di sorgenti astrofisiche, in particolare è un'analisi del SGWB fatta utilizzando dei dati sul tasso di fusione galattica per determinare delle informazioni sui meccanismi di avvicinamento dei SMBHs all'interno delle galassie risultanti alle fusioni. Per raggiungere questo scopo, è stata costruita una simulazione basata sui tassi di fusione galattica osservati e alcuni parametri che descrivono il meccanismo sconosciuto di avvicinamento dei SMBHs, alla ricerca dei valori che massimizzassero la likelihood dei modelli. I risultati sembrano favorire entrambi gli scenari, implicando che il SGWB abbia sia una componente di origine astrofisica, sia una compinente di origine cosmologica. Viene anche discussa la possibilità della presenza di una singola sorgente forte in uno dei bin, con l'aggiunta di un criterio per l'individuazione della galassia che abita.

Contents

List of Figures

List of Tables

1

Chapter 1: Introduction

1.1 Brief introduction on the subject

In the recent years different studies performed with the Pulsar Timing Array (PTA) method ultimately demonstrated the presence of a Stochastic Gravitational Wave Background (SGWB) at frequencies in the order of nHz. These works include the North American Nanohertz Observatory for Gravitational Waves (NANOGrav) (Agazie et al., 2023), the European PTA (EPTA Collaboration et al., 2023), the Parkes PTA (Zic et al., 2023) and the Chinese PTA (Xu et al., 2023). There are currently two main possibilities that are being investigated on the source of this gravitational noise, as shown in (Sesana & Figueroa, 2025): astrophyshical sources or cosmological sources.
In the astrophysical source case the SGWB is generated by a population of merging SMBHs (Phinney, 2001). Mergers between galaxies raise the question on what happends to the Super Massive Black Holes (SMBHs) living in their center once the mergers occur. The two SMBHs at the moment of the galactic merger will be at a distance $\approx 10\ kpc$, and different physical processes will bring their distance down to $\approx 10^{-5}\ pc$ (Agazie et al., 2023). Dynamical friction will bring both SMBHs to the central parts of the newly formed galaxy (Binney & Tremaine, 1987) up to a distance of a few pc. At this points the processes of stellar loss-cone scattering (Merritt, 2013) and dissipation caused by viscous drag due to circumbinary gas disks (Begelman et al., 1980) will both decrease the distance between the two SMBHs, making them a binary system with nearly circular orbit. It is important to mention that there are still a few issues in understanding how the SMBHs are brought close from a distance of a few pc to sub-pc distance: this is known in literature as the "final parsec problem" (Begelman et al., 1980); for example the loss-cone dynamic may be fueled by a low supply of stars on close orbits, and the binary would fail to merge within a Hubble time (Begelman et al., 1980), and the efficiency and the effect of the torque of the circumbinary gas disk is still unclear (Muñoz et al., 2019), (Moody et al., 2019). Even if the process is still unclear, the presence of a circumbinary gas disk seems to be in agreement with the NANOGrav data (Ellis et al., 2024a). If a binary SMBH system needs too much time to merge, there's also the possibility that the host galaxy will undergo another merger, bringing at its center another SMBH: this will greatly reduce the time needed for the three SMBHs

to come close, with also the possibility of the expulsion of the lighest SMBH from the system (Volonteri et al., 2003), (Hoffman & Loeb, 2007). Nevertheless, once the binary SMBHs are at a distance of $10^{-2} \sim 10^{-3}$ pc they will settle on an almost circular orbit and start emitting Gravitational Waves (GWs) in the nHz frequency range (Merritt et al., 2011), (Merritt, 2013). This clearly causes a lowering of the orbital energy of the system and a consequent shrinking of the orbit until the SMBHs merge (Peters & Mathews, 1963). This seems to be the more plausible source for the SGWB, as in (Ellis et al., 2024a) and (Sesana & Figueroa, 2025).

Opposed to this scenario there's the cosmological sources one: there could have been some "Beyond the Standard Model" (BSM) processes in the early Universe that could have generated this SGWB. In section 4.1 of (Sesana & Figueroa, 2025), there is an amazingly extended list of pubblication for a lot of different possibilities that we will now list: plausible cosmological causes for the SGWB could either be signals originated during inflation, after inflation but still related to inflationary set-up or signals generated after inflation and typically unrelated to the inflationary set-up; the first case includes vacuum fluctuations, strong particle production, or signals induced by large scalar fluctuations; the second case includes signals from preheating dynamics or enhanced by kination-domination; finally, the third case includes signals generated from thermal plasma motions, first order phase transitions or cosmic defects. There is also another work, (Ellis et al., 2024b), in which NANOGrav data are compared and discussed with a few of these possibilities.

In this work we assume that the astrophysical source scenario is correct, a population of merging SMBHs is the origin of the observed SGWB. We make this assumption because we aim to make some measurements about the processes that lead to the SMBHs merging: we want to see how efficient the process of SMBH merging is and also how the circumbinary gas affects the mergers; with this in mind, most of the work is based on the paper (Ellis et al., 2024a). To reach this objective we will use a multi-messanger approach, using both the SGWB NANOGrav data and a new measurement of the galactic merger rate based on the observed data of the galactic pair fraction present in literature. In particular, the data used to build our model for the SGWB are the Hellings–Downs-correlated free spectrum analysis (Hellings & Downs, 1983) of the NANOGrav data (Agazie et al., 2023), which give us the probability "violin" of observing a given SGWB signal, while the papers used for the galactic merger rate measures are (Duncan et al., 2019), (Pearson et al., 2019) and (Ventou et al., 2019). For violin, we mean that the result of the analysis of (Agazie et al., 2023) is given as the probability distribution of observed SGWB rather than with the usual average

measurement $\pm$ the 1σ Gaussian error.
This work is divided as follow: Chapter 2 describes the basis of the model and the code used in this thesis, Chapter 3 is focused on a measurement of the galactic merger rate density, Chapter 4 gives the analytical background to transform the model from depending to halo mergers to be explicitely a function of galactic mergers, Chapter 5 gives information about the code and the numerical methods used for the analysis, and finally Chapter 6 is a collection of results and comments.

2

Chapter 2: Ellis et al.'s work

2.1 Physical quantities

Every quantity in this section is expressed in geometric units $c = G = 1$.
This thesis is based on the paper (Ellis et al., 2024a) that we will now briefly summarize: the main objective of (Ellis et al., 2024a) is building a model in order to fit the measures of the Stochastical Gravitational Wave Background (SGWB from now on) performed by the NANOGrav collaboration (Agazie et al., 2023).
Given that $\rho_{GW}(f)$ is the present-day GW energy density at the observed frequency f, the NANOGrav collaboration used Pulsar Timing Array to observe a quantity $\Omega(f)$ linked to this density, the present-day GW energy density per logarithmic frequency interval divided by the rest-mass critical energy density of the Universe ρ_c (one can see its definition in eq. (2.1)).
This Ω can be expressed as a function of the properties of the sources of GW; in particular it can be linked, as in (Phinney, 2001) to the characteristics of the population of merging Super Massive Black Holes (SMBH from now on) which live at the center of all galaxies and merge as a consequence of galactic mergers

$$\Omega(f) := \frac{1}{\rho_c}\frac{d\rho_{GW}}{d\ln f} = \frac{1}{\rho_c}\int \frac{1+z}{4\pi d_L^2}\frac{dE_{GW}}{d\ln f_s}d\vec{\lambda}\,. \tag{2.1}$$

Here the integrand contains all the information regarding the sources, while the differential $d\vec{\lambda}$ contains the information on the population of SMBH; inside the integrand, $d_L(z)$ is the luminosity distance, z is redshift, $dE_{GW}/d\,ln f_s$ is the energy emitted as GW per logarithmic frequency interval in the source reference frame, while lastly f_s is the frequency of the GW in the reference frame of the source, which is related to the observed frequency f by the usual relation $f_s = (1+z)f$.
The differential $d\vec{\lambda}$ is defined as

$$d\vec{\lambda} = \frac{1}{1+z}\frac{dV_c}{dz}\frac{dR_{BH}}{d\mathcal{M}_c d\eta}d\mathcal{M}_c d\eta dz \tag{2.2}$$

where $dR_{BH}/d\mathcal{M}d\eta$ is the differential SMBH merger rate density as a function of z, the binary chirp mass $\mathcal{M}_c$ and the symmetric mass ratio η; these last two quantities are function of the two merging SMBH masses m_1 and m_2:

$$\mathcal{M}_c = \frac{(m_1 m_2)^{3/5}}{(m_1+m_2)^{1/5}} \quad , \quad \eta = \frac{m_1 m_2}{(m_1+m_2)^2} \, . \tag{2.3}$$

Since SMBH at the center of galaxies merge as a consequence of galactic mergers, the differential SMBH merger rate density can be linked to the halo mass of the merging host galaxies $M_{h,1}$ $M_{h,2}$

$$\frac{dR_{BH}}{dm_1 dm_2} = p_{merg}(m_1, m_2, z) \iint p_{occ}(m_1|M_{h,1}, z) p_{occ}(m_2|M_{h,2}, z) \frac{dR_h}{dM_{h,1} dM_{h,2}} dM_{h,1} dM_{h,2} \, , \tag{2.4}$$

where $dR_h/dM_{h,1}dM_{h,2}$ is the differential halo merger rate density (which in (Ellis et al., 2024a) is evaluated with the Extendend Press-Schechter (EPS) formalism as in (Ellis et al., 2023), (Lacey & Cole, 1993), (Erickcek et al., 2006), (Eisenstein & Hu, 1998)). In the integrand, $p_{occ}(m|M, z)$ is the probability that a SMBH with mass m lives at the center of a halo with a DM mass M at a redshift z and it was modeled as a log-normal distribution

$$p_{occ}(m|M, z) = \frac{1}{m\sigma\sqrt{2\pi}} exp\left(-\frac{\ln^2(m/\bar{m})}{2\sigma^2}\right) \, , \tag{2.5}$$

with the values of the average and the standard deviation taken from the observation of Reines & Volonteri (2015), $\sigma = 1.1$ and

$$\log_{10}\left(\frac{\bar{m}}{M_\odot}\right) = 8.95 + 1.4 \log_{10}\left(\frac{M_*}{10^{11}\, M_\odot}\right) \, . \tag{2.6}$$

Here M_* is the stellar mass that a DM halo with a mass of M_h is expected to have as found in Girelli et al. (2020)

$$M_* = 2A(z) M_h \left[\left(\frac{M_h}{M_A(z)}\right)^{-\beta(z)} + \left(\frac{M_h}{M_A(z)}\right)^{\gamma(z)}\right]^{-1} = f(M_h) \, , \tag{2.7}$$

where A, β, γ and M_A are all parameters that depend on the redshift z

$$A(z) = 0.046 \cdot (1+z)^{-0.38} \, , \qquad \log_{10} M_A(z) = 11.79 + 0.2z \, , \tag{2.8}$$

$$\beta(z) = 0.96 + 0.043z \, , \qquad \gamma(z) = 0.709 \cdot (1+z)^{-0.18} \, . \tag{2.9}$$

As explained in the appendix of (Ellis et al., 2024a), the presence of AGNs, which show to host smaller SMBH, is neglected since it's shown that their contribution to the SGWB is much smaller than that of inactive galaxies. Finally, p_{merg} is the probability that a

galactic merge produces a SMBH merging, and it will be taken either as a constant or as parameter to fit as in (Ellis et al., 2023).
In the definition eq. (2.2) the BH merger rate eq. (2.4) was transformed from being a function of the BH masses m_1 and m_2 to being a function of the binary chirp mass $\mathcal{M}_c$ and the symmetric mass ratio η provided in eq. (2.3); the inverse of equ. (2.3) are

$$m_1 = \mathcal{M}_c \frac{1+\sqrt{1-4\eta}}{2\eta^{3/5}} \quad , \quad m_2 = \mathcal{M}_c \frac{2\eta^{2/5}}{1+\sqrt{1-4\eta}} \tag{2.10}$$

.

It follows that the two differential merger rates are two forms of the same physical quantities that are linked by

$$\frac{dR_{BH}}{d\mathcal{M}_c d\eta}(\mathcal{M}_c, \eta) = \frac{\mathcal{M}_c}{\eta^{6/5}\sqrt{1-4\eta}} \frac{dR_{BH}}{dm_1 dm_2}(m_1, m_2) \ . \tag{2.11}$$

Keeping up with the quantities in eq. (2.2), dV_c/dz is the redshift rate of change of the comoving volume, which can be found, as in Carroll et al. (1992), to be

$$\frac{dV_c}{dz} = \frac{4\pi d_L^2}{H_0(1+z)^2 E_c(z)} \tag{2.12}$$

and $E_c(z)$ is the usual function found from the Friedmann equations

$$E_c^2(z) = \Omega_{\Lambda,0} + (1-\Omega_{\Lambda,0}-\Omega_{m,0})(1+z)^2 + \Omega_{m,0}(1+z)^3 \tag{2.13}$$

In this thesis the values of the cosmological parameters were chosen as $h = H_0/100\ km/s/Mpc = 0.7$, $\Omega_\Lambda = 0.73$ and $\Omega_m = 0.27$. All SMBH binary are assumed to have circular orbits as it was shown that most SMBH binaries emitting GW tipically have orbits with a very low eccentricity (Merritt, 2013), (Agazie et al., 2023) and (Ellis et al., 2023).
In their work, (Ellis et al., 2024a) assumed that the SMBH binary has another environmental mechanism other than GW emission for squeezing the orbit and losing energy, linked to the presence of gas in the vicinity of the galaxy center, creating a circumbinary gas disk, or to the loss cone orbit dynamics: since the real process for the crossing of the final parsec is still debated, generically we label all these possible mechanism as "environmental effects". (Ellis et al., 2024a) modeled the rate of change of the binary gravitational energy as a combination of the two processes of GW emission and an additional environmental energy loss

$$\dot{E} = -\dot{E}_{GW} - \dot{E}_{env} \tag{2.14}$$

each of which have its characteristic timescale

$$t_{GW} := \left| \frac{E}{\dot{E}_{GW}} \right| = 4\tau \quad , \quad t_{env} := \left| \frac{E}{\dot{E}_{env}} \right| \tag{2.15}$$

where E is the binding energy of the binary

$$E = -\frac{1}{2}(\pi f_s)^{2/3} \mathcal{M}_c^{5/3} \tag{2.16}$$

and τ is its coalescence time

$$\tau = \frac{5}{256}(\pi f (1+z))^{-8/3} \mathcal{M}_c^{-5/3} \ . \tag{2.17}$$

Considering both energy loss processes, (Ellis et al., 2024a) were able to describe the rate of change of the frequency of the emitted GW in the source reference frame

$$\frac{d \ln f_s}{dt} = \frac{3}{2} t_{GW}^{-1} \left(1 + \frac{t_{GW}}{t_{env}} \right) \tag{2.18}$$

and the GW spectrum from an inspiring binary as

$$\frac{dE_{GW}}{d \ln f_s} = \frac{1}{3} \frac{(\pi f_s)^{2/3} \mathcal{M}_c^{5/3}}{1 + t_{GW}/t_{env}} \tag{2.19}$$

Since the environmental time scale t_{env} is unknown, (Ellis et al., 2024a) chose to write the series expansion of $\ln(t_{env}/t_{GW})$ in $\ln f_s$ and approximate it at the leading order as

$$\frac{t_{env}}{t_{GW}} \approx \left(\frac{f_s}{f_{GW}} \right)^{\alpha_{PW}} \tag{2.20}$$

where α_{PW} is an unknown parameter and f_{GW} is a characteristic frequency above which GW emission becomes dominant (i.e. the SMBH becomes closer and closer) and is described as another power-law with a new fit parameter f_{ref}

$$f_{GW} = f_{ref} \left(\frac{\mathcal{M}_c}{10^9 \ M_\odot} \right)^{-0.4} \tag{2.21}$$

so the model itself has three fit parameters that we combine in the vector $\vec{\theta}_M = (p_{merg}, \alpha_{PW}, f_{ref})$.

2.2 Probability of a model and results

The GW background eq. (2.1) that (Ellis et al., 2024a) used to measure the parameters p_{merg}, α_{PW} and f_{ref} is mainly the result of $\mathcal{O}(100)$ of strong sources emitting the main

part of it (see (Agazie et al., 2023) and (Ellis et al., 2023)), so in (Ellis et al., 2024a) the authors generated Monte Carlo realizations of the SGWB in each NANOGrav frequency bin up to $f = 30\ nHz$ as the contribution of all the individual signals $\Omega^{(1)}(\vec{\theta}_b)$ coming from each SMBH binaries source

$$\Omega(f_i) = \frac{1}{\ln(f_{i+1}/f_i)} \sum_{k=1}^{N(f_i)} \Omega^{(1)}(\vec{\theta}_b^k) \tag{2.22}$$

where the vector $\vec{\theta}_b = (f, \mathcal{M}, \eta, z)$ contains the parameters of the binary emitter, while we sum over $N(f_i)$ number of sources expected at the frequency bin $[f_i,\ f_{i+1}]$; since we aim to generate Monte Carlo realizations of Ω, for each one of these realizations the number of sources N in eq. (2.22) should be extracted from a Poisson distribution with an average value corresponding to the expected number of sources

$$\bar{N}(f_i) = \iint_{f\in[f_i,f_{i+1}]} d\vec{\lambda} d\tau \tag{2.23}$$

If we assume that no binary changes bin during the period of measurement of Ω, (a reasonable assumption since the typical timescales for SMBH mergers are really much longer than the period of observation of NANOGrav of 16.3 years), then (Ellis et al., 2023), (Ellis et al., 2024a) showed that each one of the individual signals $\Omega^{(1)}(\vec{\theta}_b)$ generated in the sum of eq. (2.22) is extracted from a probability distribution proportional to

$$P^{(1)}(\Omega|f, \vec{\theta}_M) \propto \int \delta(\Omega - \Omega^{(1)}) \left| \frac{dt}{d\ln f_s} \right| d\vec{\lambda} \tag{2.24}$$

where the expression $dt/d\ln f_s$ is the inverse of eq. (2.18) and each source with parameters $\vec{\theta}_b = (f, \mathcal{M}_c, \eta, z)$ produces a GW signal

$$\Omega^{(1)}(\vec{\theta}_b) = \frac{1}{\rho_c} \frac{1+z}{4\pi d_L^2} \frac{dE_{GW}}{dt} = \frac{8(1+z)}{5\pi\rho_c d_L^2} (\pi f(1+z)\mathcal{M}_c)^{10/3} \tag{2.25}$$

There should be a dependence on the inclination angle in the integral (2.24), but, as shown in (Ellis et al., 2023), including it for each binary or just using an average value does not change the results. One could expect that the number of binaries present in each bin would be very large, so that the probability distribution of the total signal $P(\Omega|f_i, \vec{\theta}_M)$ converges to a Gaussian, but in the same paper (Ellis et al., 2023) it was shown that the probability distribution for each source $P^{(1)}(\Omega|f_i, \vec{\theta}_M)$ has a long tail $P \propto \Omega^{-2.5}$ at high values of Ω which prevents the central limit theorem from helping us. This tail is generated by a limited number of the strongest binaries and since it can take

a lot of time to generate it with a Monte Carlo approach, we deal with it in a different way.
The generated GW signal eq. (2.22) is split into a strong and a weak part, which will be treated differently

$$\Omega = \Omega_S + \Omega_W \tag{2.26}$$

We discriminate between strong and weak parts by assuming that in the strong term (the first one) we only consider the N_S sources with a signal above a given threshold $\Omega > \Omega_{th}$ that we will soon fix. The signal generated by strong sources is the sum of N_S signals from individual strong sources

$$\Omega_S(f_i) = \frac{1}{\ln(f_{i+1}/f_i)} \sum_{k=1}^{N_S(f_i)} \Omega_S^{(1)}(\vec{\theta}_b^k) \tag{2.27}$$

This is a sum of identical random variables each with a probability distribution

$$P_S^{(1)}(\Omega) = \frac{1}{p_S}\Theta(\Omega - \Omega_{th})P^{(1)}(\Omega) \tag{2.28}$$

where Θ is the usual Heaviside function, while p_S is just the probability of finding a strong source, i.e. a source with a signal strength bigger than Ω_{th}

$$p_S := \int_{\Omega>\Omega_{th}} P^{(1)}(\Omega)d\Omega \tag{2.29}$$

The expected number of strong sources is then

$$\tilde{N}_S = p_S\tilde{N} \tag{2.30}$$

since we have only a small number of strong sources, we can just choose to fix an arbitrary number of strong sources but with the costraint that $\bar{N}_S \ll \bar{N}$, which means $p_S \ll 1$.
All of this means that to obtain a strong signal (Ellis et al., 2024a) generated $\bar{N}_S = 50$ strong sources, summed their contribution as in eq. (2.27) and repeated this process $4 \cdot 10^5$ times in each bin to obtain a sample of the strong signals; this set of strong signals was then used to find its continuous probability distribution $P_S(\Omega)$.
For high-enough values of Ω_S, typically for $\Omega_S \gtrsim 10^{-9}$, the probability of finding a source becomes extremely small, so that Monte Carlo realization in these range becomes unreliable and really time consuming: it can be shown (Ellis et al., 2024a) that in this range of signals the probability of observing a total signal Ω can be approximated

analytically with

$$P(\Omega) \approx \bar{N} \ln\left(\frac{f_{i+1}}{f_i}\right) P^{(1)}\left(\ln\left(\frac{f_{i+1}}{f_i}\right)(\Omega - \bar{\Omega})\right) \tag{2.31}$$

where of $\bar{\Omega}$ is the average signal measured.
Following the same reasoning, the signal generated by weak sources is

$$\Omega_W(f_i) = \frac{1}{\ln(f_{i+1}/f_i)} \sum_{k=1}^{N_W(f_i)} \Omega_W^{(1)}(\vec{\theta}_b^k) \ , \tag{2.32}$$

each weak source has a probability distribution

$$P_W^{(1)}(\Omega) = \frac{1}{1-p_S}\Theta(\Omega_{th} - \Omega)P^{(1)}(\Omega) \ , \tag{2.33}$$

and the expected number of weak sources is

$$\bar{N}_W = (1-p_S)\bar{N} \approx \bar{N} \gg \bar{N}_S \ . \tag{2.34}$$

Since the number of weak sources can be extremely high and their probability distribution does not possess a long tail, the authors exploited the central limit theorem, so that the probability distribution of the weak sources is a Gaussian distribution

$$P_W(\Omega) = \frac{1}{\sigma_W\sqrt{2\pi}} \exp\left(-\frac{(\Omega - \bar{\Omega}_W)^2}{2\sigma_W^2}\right) \tag{2.35}$$

where its average and standard deviation can be written as

$$\bar{\Omega}_W = \int_{\Omega \leq \Omega_{th}} \Omega P^{(1)}(\Omega) d\Omega \approx \tag{2.36}$$

$$\approx \frac{1}{\ln(f_{i+1}/f_i)} \int_{f\in[f_i,f_{i+1}]} d\ln f \int_{\Omega^{(1)}\leq\Omega_{th}} \Omega^{(1)} \left|\frac{dt}{d\ln f_s}\right| d\vec{\lambda} \tag{2.37}$$

$$\sigma_W = \frac{\sqrt{N_W}}{\ln(f_{i+1}/f_i)} \sqrt{\left\langle \left(\Omega_W^{(1)}\right)^2 \right\rangle - \left\langle \Omega_W^{(1)} \right\rangle^2} \tag{2.38}$$

Finally, the probability distribution of measuring Ω in the bin $[f_i, f_{i+1}]$ with a given model $\vec{\theta}_M$ is

$$P_{model}(\Omega|f_i, \vec{\theta}_M) = \int P_W(\Omega - \Omega')P_S(\Omega')d\Omega' \approx P_S(\Omega - \bar{\Omega}_W) \ , \tag{2.39}$$

where the last approximation holds since P_W is much narrower than P_S (σ_W is really

small), mimicking a Dirac delta distribution. The likelihood of a model with parameters $\vec{\theta}_M$ will be proportional to

$$\mathcal{L}(\vec{\theta}_M) \propto \prod_i \int P_{data}(\Omega|f) P_{model}(\Omega|f_i, \vec{\theta}_M)\, d\Omega\ ; \tag{2.40}$$

in order to compare different models and hypothesis, (Ellis et al., 2024a) defined the likelihood ratio

$$\mathcal{R} = \frac{max_{\vec{\theta}_M} \mathcal{L}(\vec{\theta}_M|H_1)}{max_{\vec{\theta}_M} \mathcal{L}(\vec{\theta}_M|H_2)} \tag{2.41}$$

where the two compared hypothesis are the presence or not of the environmental effects. The GW-driven model H_1 (modeled with $f_{ref} \to 0$) has as a unique parameter p_{merg}, with a best fit value of 0.44, while the mixed model H_2 produced a higher likelihood for the best-fit values $p_{merg} = 0.85$, $\alpha_{PW} = 2$ and $f_{ref} \approx 34\ nHz$. Their likelihood is shown in fig. 2.1

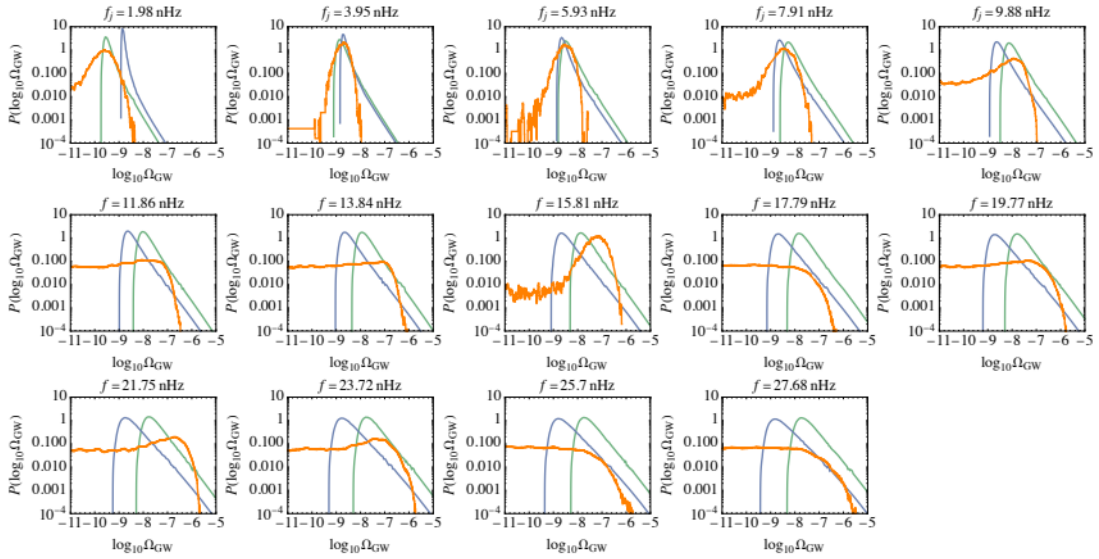

Figure 2.1. The distributions of the posterior probability in the 14 NANOGrav frequency bins for the best fit points with (green) and without (blue) the environmental effects for the model described in (Ellis et al., 2024a). The orange curves show the NANOGrav violin data.

3

Chapter 3: Observed merger rate

The aim of this work is to improve the model of (Ellis et al., 2024a), with the inclusion of another set of data together with the NANOGrav ones: instead of using a theoretical halo merger rate, like the one predicted by the EPS formalism, we want to use observed galactic merger rates. We would be lucky if someone measured the differential halo merger rate density but unfortunately for us most literature works focus on measuring a different quantity, the total galactic merger rate density $\Gamma_{tot}(z)$; if we call $dR_{gal}/dM_* d\mu$ the differential galactic merger rate density, these two quantities will be linked by an integral:

$$\Gamma_{tot}(z) = \int_0^\infty dM_* \int_0^1 \frac{dR_{gal}}{dM_* d\mu} d\mu \tag{3.1}$$

where for each pair of merging galaxies M_* is the stellar mass of the heavier one, while μ is the ratio between the mass of the lighter and the mass of the heavier. One should be warned that the differential galactic merger rate density and the halo merger rate density are two different quantities, which are clearly linked but are not the same. There are a lot of works in literature that measure this quantity, but they usually obtain only the major merger rate density for the heaviest galaxies, lacking all the information about minor mergers or light galaxies: this is because light galaxies are faint and could be lost in the measure of $\Gamma_{tot}(z)$, making the observed value an underestimation of the real one.

3.1 The datasets and the analysis

We want to obtain the most comprehensive measure of $\Gamma_{tot}(z)$ possible, and in order to do so we will do it following the methods of (Duncan et al., 2019) and (Conselice et al., 2022): we will recover in literature the measurement of the galactic pair fraction f_{pair} at different redshift, and then convert them into a galactic merger rate density as in (Duncan et al., 2019)

$$\Gamma(z;\, M_* > M_{th}\,,\, \mu > \mu_{th}) = \frac{n_*(M_* > M_{th}, z) \cdot f_{pair}(\mu > \mu_{th})}{\tau_{merge}(z)}\,. \tag{3.2}$$

The arguments other than z from which Γ depends remind of the minimum mass and mass ratio used in the measure; the quantity $n_*(M > M_{th})$ is the total number density of galaxies with a mass above the threshold one, and comes from the fit Schechter function from (Mortlock et al., 2015), $\tau(z)$ is the estimated merger timescale given the redshift, and finally the quantity f_{pair} is just the pair fraction measured for mergers with a mass ratio μ above a given threshold μ_{th}.
One could see that the measured galactic merger rate density eq. (3.2) is a function of the differential galactic merger rate density, but with other lower integral boundaries than eq. (3.1):

$$\Gamma(z;\, M_* > M_{th}\,,\, \mu > \mu_{th}) = \int_{M_{th}}^{\infty} dM_* \int_{\mu_{th}}^{1} \frac{dR_{gal}}{dM_* d\mu} d\mu\ . \tag{3.3}$$

We will limit ourselves in measuring the total merger rate density for redshifts $z < 3$, for two main reasons:

- as we look at higher and higher redshifts, the minimum luminosity that a source must have to be detected increases, making the number of observed galaxies an underestimation of the real value, and the observed pair fraction will be based on an incomplete sample (Duncan et al., 2019);
- a distributions of the binary parameters for a sampling of SMBHs binary population was generated in (Ellis et al., 2023), and it was found that the PTA SGWB signal is dominated by events happening in the redshift range $1 \lesssim z \lesssim 3$;

Together with completeness issues there is also another reason why works that measure $\Gamma_{tot}(z)$ typically consider only the major mergers while ignoring the minor ones and it has to do with the uncertainties on the merger timescale $\tau(z)$; to overcome this problem, this work assumes the $\mu-$dependent timescale found in (Conselice et al., 2022), which is based on the ILLUSTRIS Simulation (Snyder et al., 2017)

$$\tau_{merge}(\mu, z) = (2.06 - 0.65\mu)(1+z)^{-1.6}\ Gyr\ . \tag{3.4}$$

If we want to use this $\mu-$dependent timescale, we must modify eq. (3.2): we can upgrade it for it to consider different merger timescales by writing it as an integral:

$$\Gamma(z;\, M_* > M_{th}\,,\, \mu > \mu_{th}) = \frac{n_*(M_* > M_{th}, z)}{1-\mu_{th}} \int_{\mu_{th}}^{1} \frac{f_{pair}(\mu)}{\tau_{merge}(\mu, z)} d\mu \tag{3.5}$$

one can see that if we remove the dependence of μ from the denominator, we recover the old measure eq. (3.2). What we need now are just the data of the observed pair

fraction, and we will take them from 3 articles so that we can span different values for both masses of the merging galaxies:

- we take the results of (Duncan et al., 2019), who measured the total pair fraction for galaxies with masses $\log_{10}(M_*/M_\odot) > 9.7$ and redshifts $0.5 \leq z \leq 3$ in the CANDELS field, obtaining as a result the fit

$$F_{cum}(>\mu) = A\left(\frac{1}{\mu} - 1\right)^B \tag{3.6}$$

  This total pair fraction is normalized considering only mergers with $1/20 < \mu < 1$, and the values of the fit parameters A and B can be found in table (3.1). Since this is a cumulative distribution, it is pretty straightforward to recover the pair distribution itself, we just have to use to notice that these two functions are linked as

$$F_{cum}(>\mu) = \int_\mu^1 f_{pair}(\mu')d\mu' \tag{3.7}$$

  and use the fundamental theorem of calculus to express the pair distribution as

$$f_{pair}(\mu) = \frac{dF_{cum}}{d\mu} = \frac{AB}{\mu^2}\left(\frac{1}{\mu} - 1\right)^{B-1} \tag{3.8}$$

  this function is then integrated in eq. (3.5) to obtain the merger rates.

- we take the results of (Ventou et al., 2019), who measured the pair fraction with the Multi-Unit Spectroscopic Explorer (MUSE) deep observations over the Hubble Deep Field South, COSMOS-Gr30, and Abell 2744 regions. This work measured both the major ($\mu > 1/4$) and minor ($1/100 < \mu < 1/4$) pair fraction, but on two different mass ranges: the major merger measure spans galaxy masses $7 \leq \log_{10}(M_*/M_\odot) \leq 11$, while the minor merger measure just spans galaxy masses $9 \leq \log_{10}(M_*/M_\odot) \leq 11$; all galaxies considered in this work are in a redshitf range $0.2 \leq z \leq 6$; we are lacking all the information about galaxies heavier than $\log_{10}(M_*/M_\odot) = 11$ but due to the power-law nature of the distribution of galaxies (Mortlock et al., 2015) most of the galaxies have low mass, hence the mass range considered in (Ventou et al., 2019) makes up the most contribution to the merger rate density; we only took the data from the redshift bins from which both the major and minor pair fractions were known;

z	$\log_{10} A$	B	$\Gamma_{tot}(z)$ $[10^{-4}\ Mpc^{-3}\ Gyr^{-1}]$
0.75	-1.472 ± 0.040	0.413 ± 0.042	10.8 ± 7.1
1.25	-1.522 ± 0.039	0.540 ± 0.040	15.9 ± 9.6
1.75	-1.291 ± 0.033	0.515 ± 0.041	17.4 ± 5.4
2.25	-1.299 ± 0.051	0.491 ± 0.078	16.5 ± 8.3
2.75	-1.346 ± 0.078	0.582 ± 0.160	20.1 ± 15.7

Table 3.1. This table shows the redshift z of the pair fraction measures of (Duncan et al., 2019), the corresponding best fit values for the parameters A and B of eq. (3.8), and the corresponding total galactic merger rate density Γ_{tot}. The measured pair fraction here considered only mergers in the range $1/20 < \mu < 1$

- we take the results of (Pearson et al., 2019), which measured the pair fraction in the SDSS, KiDS and again in the CANDELS imaging surveys, but with a different method than (Duncan et al., 2019) training a neural network to recognize mergers; the galaxies for which the pair fraction was measured had redshifts $0 \leq z \leq 4$; each of the different data sets spans different values of masses, always from a low-mass threshold and going up;

All the pair fraction values used with the corresponding errors can be found in table (3.2).
Despite the fact that among the three papers the measurements of the pair fractions were performed among different mass ranges, we assume that the measured pair fraction is the same that one would measure in the mass range $\log_{10}(M_*/M_\odot) > 9.7$, so that the minimum galactic mass in the number density of eq. (3.5) can be taken as $10^{9.7}\ M_\odot$ for all works; this value was chosen in order to have consistency between the different measures of the galactic merger rate density; moreover, the data listed in (Ventou et al., 2019) seem to suggest that the measure of pair fraction are consistent among different mass bins for a population of galaxies at the same redshift bin.
Now that we have collected the data of the observed galactic merger rate density, we assume a model for it such that its shape is the same as in (Conselice et al., 2022):

$$\Gamma_{tot}(z\ ;\ M_* > M_{th}) = \Sigma(1+z)^{\tau} \exp(\upsilon z) \tag{3.9}$$

3.2 The measured merger rate density

Given the data Γ_{data} evaluated at each redshift z_i and their associated error $\sigma(z_i)$, the best fit values were found as the values of (Σ, τ, υ) that maximize the logarithm of the likelihood

Paper origin	z	f_{pair}	μ range	$\Gamma_{tot}(z)$ $[10^{-4}\ Mpc^{-3}\ Gyr^{-1}]$
(Ventou et al., 2019)	0.60	0.078 ± 0.039	[0.25, 1.00]	5.9 ± 1.7
		0.199 ± 0.053	[0.01, 0.25]	
	1.23	0.127 ± 0.079	[0.25, 1.00]	8.3 ± 3.6
		0.196 ± 0.086	[0.01, 0.25]	
	2.15	0.172 ± 0.111	[0.25, 1.00]	5.9 ± 3.6
		0.129 ± 0.061	[0.01, 0.25]	
(Pearson et al., 2019)	0.053	0.141 ± 0.013	[0, 1]	0.76 ± 0.22
	0.075	0.300 ± 0.043	[0, 1]	0.17 ± 0.75
	0.300	0.320 ± 0.068	[0, 1]	2.4 ± 3.5
	0.725	0.322 ± 0.068	[0, 1]	3.8 ± 3.9
	1.030	0.326 ± 0.069	[0, 1]	5.0 ± 3.3
	1.435	0.378 ± 0.080	[0, 1]	7.8 ± 5.2
	2.830	0.421 ± 0.089	[0, 1]	17.9 ± 3.8

Table 3.2. This tables shows the data used in the analysis, in particular the first column divides the used data in their corresponding origin, the second column gives the redshift of each pair measure, the third column tells the pair fraction data used, the fourth column tells us among which values of μ the measure was perfomed (to discriminate between major and minor mergers), while the fourth column gives the corresponding measured galactic merger rate density

$$\ln \mathcal{L}_{merge} = -\frac{1}{2} \sum_{z_i} \left(\frac{\Gamma_{data}(z_i) - \Gamma_{model}(z_i; \Sigma, \tau, \upsilon)}{\sigma(z_i)} \right)^2 . \tag{3.10}$$

The results were found with the python module `emcee` (Foreman-Mackey et al., 2013), generating a distribution for the likelihood having its maximum value for the parameters

$$\log_{10} \left[\frac{\Sigma}{Mpc^{-3}\ Gyr^{-1}} \right] = -4.22^{+0.12}_{-0.15} \quad , \quad \tau = 5.50^{+1.68}_{-1.65} \quad , \quad \upsilon = -1.50^{+0.79}_{-0.81} . \tag{3.11}$$

The best fit curve can be seen in fig. 3.1 and compared both with the obtained galactic merger rate density measures and the corresponding merger rate density expected from the EPS formalism of the previous chapter: the data seem to suggest a slightly lower merger rate density for low redshift, while a $10\times$ larger merger rate density than expected at high redshift. In fig. 3.2 we can see the contours for the fit parameters, with a strong correlation between the power-law index τ and the exponential coefficient υ.

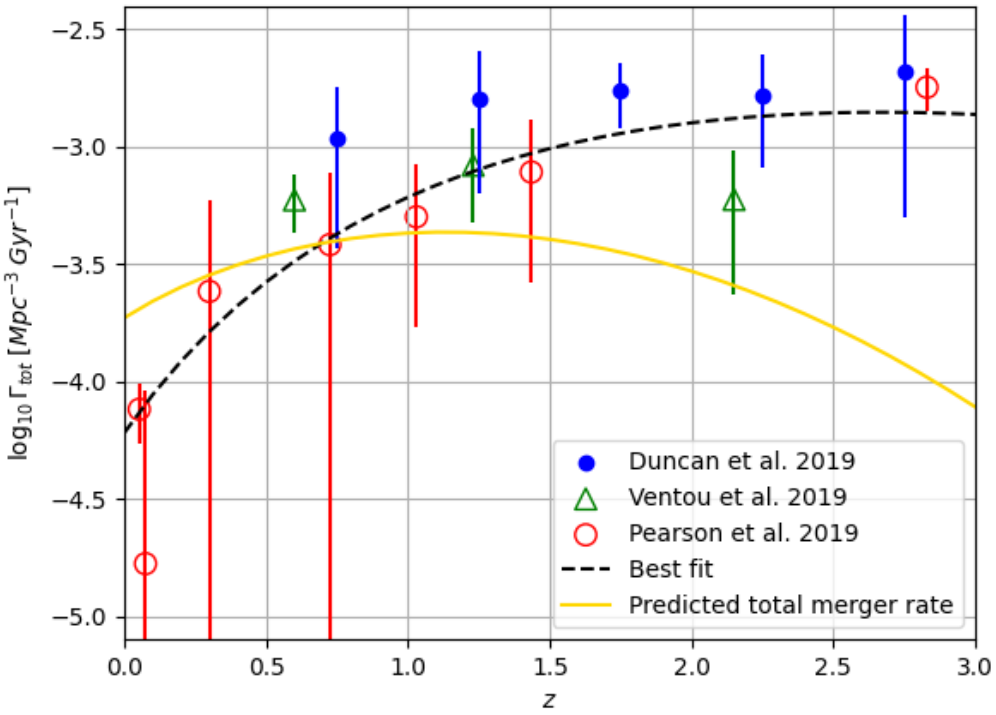

Figure 3.1. All the resulting galactic merger rate density divided accordingly from their data's paper of origin. We also plot the best fit curve eq. (3.9) with parameters eq. (3.11) and the corresponding galactic merger rate density predicted from the EPS formalism with $\log_{10}(M_{th}/M_{\odot}) = 9.7$ and $\mu > 0$.

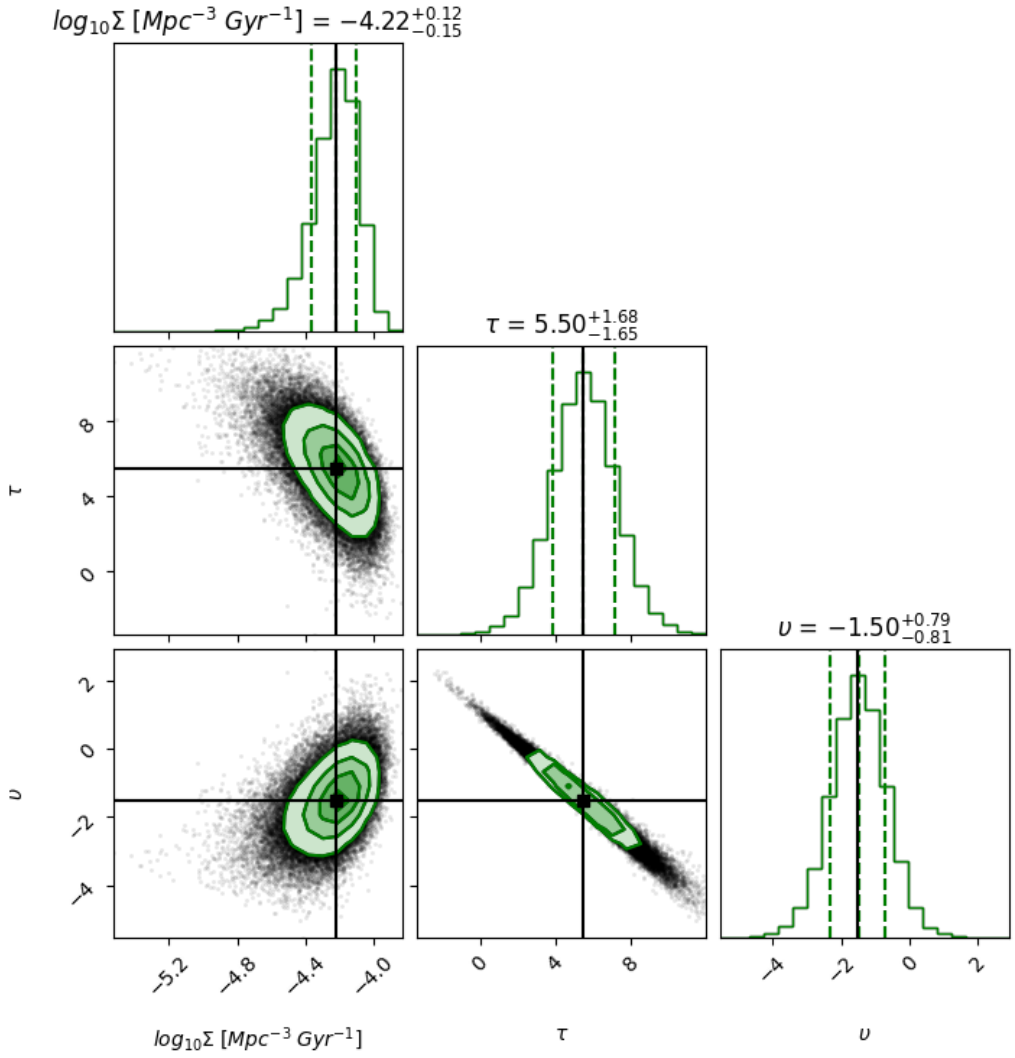

Figure 3.2. Contour plot for the parameters of the best fit eq. (3.9)

4

Chapter 4: Including the observed galaxy merger rate

We need to find a way of using the observed merger rate density to create a model that emulates the NANOGrav data. If we look at the equations listed in the second chapter it means acting on equ. 2.4, and writing it so that it is a function of the observed *total galactic* merger rate density rather than the theoretical EPS *differential DM halo* merger rate density

$$\frac{dR_h}{dM_{h,1}dM_{h,2}}(M_{h,1}, M_{h,2}, z) \rightarrow \Gamma_{tot}(z) \tag{4.1}$$

We then have two objectives:

- find a relation between the galactic quantities (linked to the stellar mass content of galaxies) and the halo quantities (linked to the DM mass content of galaxies);
- find a way for working with the total merger rate density rather that with the differential merger rate density

This chapter is enterely focused on reaching these two goals.

4.1 From DM to stellar masses

We need to rewrite the formalism of eq. (2.4) so that the integral is performed over stellar masses $M_{*,1}$ and $M_{*,2}$ of the merging galaxies instead of being evaluated over their DM halo masses $M_{h,1}$ and $M_{h,2}$. First of all, we define some integration boundaries:

$$\frac{dR_{BH}}{dm_1 dm_2} = \frac{p_{merg}}{2} \iint_S p_{occ}(m_1|f(M_{h1}), z) p_{occ}(m_2|f(M_{h2}), z) \frac{dR_h}{dM_{h1}dM_{h2}} dM_{h1} dM_{h2} \ . \tag{4.2}$$

The regions over which this integrals is evaluated is $S = (\mathbb{R}^+ \times \mathbb{R}^+)$ which correspond to the positive quadrant of the (M_{h1}, M_{h2}) plane; the factor $1/2$ was inserted since this integral is counting over all SMBH mergers twice. We then redefine the BH merger rate making it a function of the stellar masses of the merging galaxies instead of a function of their DM masses:

$$\frac{dR_{BH}}{dm_1 dm_2} := \frac{p_{merg}}{2} \iint_S p_{occ}(m_1|M_{*1}, z) p_{occ}(m_2|M_{*2}, z) \frac{dR_{gal}}{dM_{*1} dM_{*2}} dM_{*1} dM_{*2} \ ; \quad (4.3)$$

again, the factor 1/2 was inserted because in the integration all galactic mergers are counted twice. These two definitions (eq. (4.2) and eq. (4.3)) are clearly linked and we aim to change the integration variable $M_h \to M_*$, but in order to do so we need to find the inverse function f^{-1} of the function linking the stellar mass and the DM mass of a galaxy eq. (2.7); the problem is that in general f does not have an analytical inverse. So we will build an approximation of f^{-1} as follows: as can be see in fig, 4.1, f^{-1}, which was plotted by just swapping the values of M_h and M_*, almost behaves like the sum of two different power laws. We then supposed that it actually *is* a sum of power laws in the form

$$M_h = f^{-1}(M_*) := B \left(\frac{M_*}{M_A}\right)^C \left[1 + D \left(\frac{M_*}{M_A}\right)^E\right] , \quad (4.4)$$

where all the unknown quantities B, C, D and E are only functions of the redshift. We then focus on the behaviour of this inverse at the limits of its domain: since we know that the higher the DM content of a halo, the higher the stellar mass content, we can say that when M_h is small, M_* is also small, and the same goes on for when they are large. We can approximate both functions by using simple power laws at these limits

$$f(M_h) \xrightarrow[M_h \to 0]{} 2AM_A \left(\frac{M_h}{M_A}\right)^{1+\beta} \qquad f(M_h) \xrightarrow[M_h \to \infty]{} 2AM_A \left(\frac{M_h}{M_A}\right)^{1-\gamma}$$
$$f^{-1}(M_*) \xrightarrow[M_* \to 0]{} B \left(\frac{M_*}{M_A}\right)^C \qquad f^{-1}(M_*) \xrightarrow[M_* \to \infty]{} BD \left(\frac{M_*}{M_A}\right)^{C+E}$$

and now we impose that $f^{-1}(f(M_h)) = M_h$ so that we can find the unknown constants in eq. (4.4); it follows that the inverse of f is approximately equal to

$$M_h = f^{-1}(M_*) \approx M_A \left(\frac{M_*}{2AM_A}\right)^{C(z)} \left[1 + \left(\frac{M_*}{2AM_A}\right)^{E(z)}\right] , \quad (4.5)$$

with the new parameters linked to the old ones as

$$C(z) = \frac{1}{\beta(z) + 1} \ , \ E(z) = \frac{\beta(z) + \gamma(z)}{(1 + \beta(z))(1 - \gamma(z))} . \quad (4.6)$$

This is not the exact inverse, but as can be seen in fig. 4.1, the maximum deviation

from the true inverse function is negligible for our purposes.

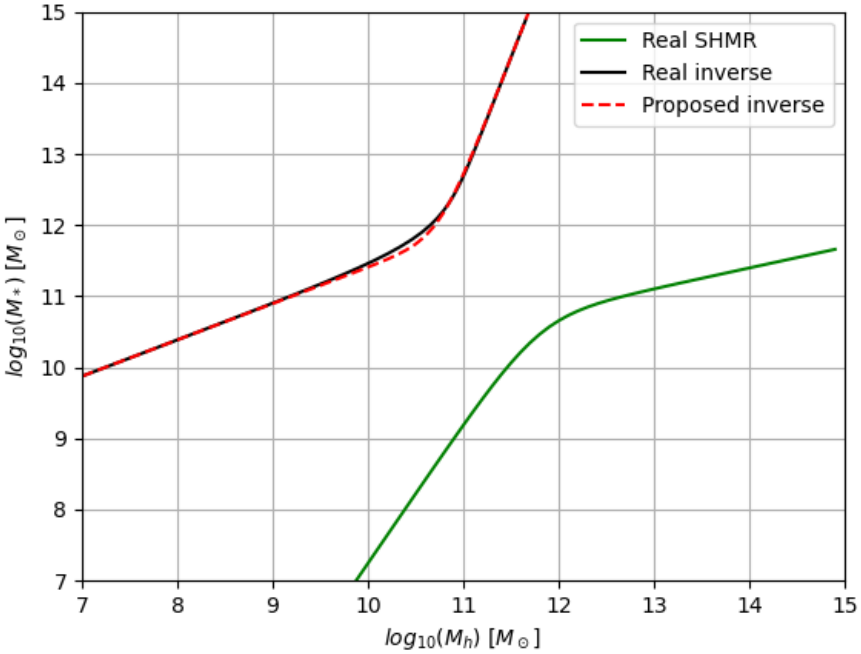

Figure 4.1. The real SHMR as found in (Girelli et al., 2020), its real inverse function and the proposed pseudo-inverse function eq. (4.4) are plotted here. The difference between the real (numerically computed) inverse and the proposed analytical inverse is negligible for our purposes.

We apply the said change of variable $M_h \to M_*$ at eq. (4.2): it can be shown that the determinant of the transformation is

$$detJ(M_{*1}, M_{*2}) = \left(\frac{C}{2A}\right)^2 \left(\frac{M_{*1}}{2AM_A} \cdot \frac{M_{*2}}{2AM_A}\right)^{C-1} \times \\ \times \left[1 + \frac{1+\beta}{1-\gamma}\left(\frac{M_{*1}}{2AM_A}\right)^E\right]\left[1 + \frac{1+\beta}{1-\gamma}\left(\frac{M_{*2}}{2AM_A}\right)^E\right] \quad (4.7)$$

,

so that

$$\frac{dR_{BH}}{dm_1 dm_2} = \frac{p_{merg}}{2} \iint_S p_{occ}(m_1|M_{*1}) p_{occ}(m_2|M_{*2}) \times \\ \times \frac{dR_h(f^{-1}(M_{*1}), f^{-1}(M_{*2}))}{dM_{h1} dM_{h2}} detJ(M_{*1}, M_{*2}) dM_{*1} dM_{*2} \ . \quad (4.8)$$

We now compare this result with eq. (4.3) and we find that the two differential merger rate densities are linked as

$$\frac{dR_{gal}(M_{*1}, M_{*2})}{dM_{*1} dM_{*2}} = detJ(M_{*1}, M_{*2}) \frac{dR_h(f^{-1}(M_{*1}), f^{-1}(M_{*2}))}{dM_{h1} dM_{h2}} \ . \quad (4.9)$$

this will come in handy later.

4.2 From (M_{*1}, M_{*2}) to (M_*, μ)

We want to perform another variable change to the integral, from the stellar masses $M_{*,1}$ and $M_{*,2}$ of the merging galaxies to the mass M_* of the more massive one and the mass ratio μ of the pair:

$$M_* = M_{*1} \ , \ \mu = \frac{M_{*2}}{M_{*1}} \ . \quad (4.10)$$

The determinant of the Jacobian F for this transformation is simply

$$detF(M_*, \mu) = \begin{vmatrix} \frac{\partial M_{*1}}{\partial M_*} & \frac{\partial M_{*1}}{\partial \mu} \\ \frac{\partial M_{*2}}{\partial M_*} & \frac{\partial M_{*2}}{\partial \mu} \end{vmatrix} = \begin{vmatrix} 1 & 0 \\ \mu & M_* \end{vmatrix} = M_* \quad (4.11)$$

so eq. (4.3) becomes

$$\frac{dR_{BH}}{dm_1 dm_2} = \frac{p_{merg}(m_1, m_2, z)}{2} \iint_S p_{occ}(m_1|M_*) p_{occ}(m_2|\mu M_*) \times \\ \times \frac{dR_{gal}(M_*, \mu M_*, z)}{dM_{*1} dM_{*2}} detF(M_*, \mu) dM_* d\mu \quad (4.12)$$

If we apply again the idea of giving a new definition to the galactic merger rate that let us rewrite eq. (4.2) into eq. (4.3), we can say that the BH merger rate is expressed as a function of M_* and μ as

$$\frac{dR_{BH}}{dm_1 dm_2} = \frac{p_{merg}(m_1, m_2, z)}{2} \iint_S p_{occ}(m_1|M_*) p_{occ}(m_2|\mu M_*) \frac{dR_{gal}}{dM_* d\mu} dM_* d\mu \tag{4.13}$$

because the two differential merger rate densities are related as

$$M_* \frac{dR_{gal}(M_*, \mu M_*, z)}{dM_{*1} dM_{*2}} = \frac{dR_{gal}(M_*, \mu, z)}{dM_* d\mu} \, . \tag{4.14}$$

4.3 Observed and predicted rates

All of this work was needed to show that we can indeed write eq. (4.2) into a form which is more suitable for the observational data provided in the previous chapter. In fact, one can recognize that the fit provided in eq. (3.9) can be linked to the galactic merger rate obtained in eq. (4.13)

$$\Gamma_{tot}(z \, ; \; M_* > 10^{9.7} \, M_\odot) = \int_0^1 d\mu \int_{10^{9.7} M_\odot}^\infty \frac{dR_{gal}}{dM_* d\mu} dM_* \tag{4.15}$$

We now need to find a smart way in which we can write eq. (4.13) so that the region upon which the integral is performed coincides with that of eq. (4.15). First, we get rid of all the mergers with $\mu > 1$: for the sake of brevity, we define

$$I(m_1, m_2, M_*, \mu, z) := p_{merg}(m_1, m_2, z) p_{occ}(m_1|M_*) p_{occ}(m_2|\mu M_*) \frac{dR_{gal}(M_*, \mu, z)}{dM_* d\mu} \tag{4.16}$$

We then recall the definition of $S = (\mathbb{R}^+ \times \mathbb{R}^+)$, the region over which the BH merger rate density eq. (4.13) is evaluated; we split this integral over two areas, T and $S \setminus T$, such that $T = (\mathbb{R}^+ \times [0, 1])$

$$\frac{dR_{BH}}{dm_1 dm_2} = \frac{1}{2} \left[\int_0^1 d\mu \int_0^\infty I \, dM_* + \int_1^\infty d\mu \int_0^\infty I \, dM_* \right] \tag{4.17}$$

We want to integrate on T only, so we do another change of variable in the second integral, the one with domain of integration $S \setminus T$

$$M_*' = \mu M_* \, , \; \mu' = \frac{1}{\mu} \tag{4.18}$$

this transformation just swaps the masses of the two merging galaxies; the determinant of the Jacobian G of this transformation is

$$|detG(M'_*, \mu')| = \begin{vmatrix} \frac{\partial M_*}{\partial M'_*} & \frac{\partial M_*}{\partial \mu'} \\ \frac{\partial \mu}{\partial M'_*} & \frac{\partial \mu}{\partial \mu'} \end{vmatrix} = \begin{vmatrix} \mu' & M'_* \\ 0 & -\frac{1}{\mu'^2} \end{vmatrix} = \frac{1}{\mu'} \tag{4.19}$$

hence the integral over $S \setminus T$ in eq. (4.17) becomes

$$\iint_T p_{merg} p_{occ}(m_1|\mu' M'_*) p_{occ}(m_2|M'_*) \frac{1}{\mu'} \frac{dR_{gal}(\mu' M'_*, 1/\mu', z)}{dM_* d\mu} dM'_* d\mu'$$

and we underline how this transformation made the area of integration become T. Now, we exploit a symmetry of the differential galactic merger rate $dR_{gal}/dM_{*1}dM_{*2}$: this quantity must be invariant for the exchange of the two masses of the merging galaxies

$$\frac{dR_{gal}(M_{*1}, M_{*2})}{dM_{*1}dM_{*2}} = \frac{dR_{gal}(M_{*2}, M_{*1})}{dM_{*1}dM_{*2}} \implies \frac{dR_{gal}(M_*, \mu M_*)}{dM_{*1}dM_{*2}} = \frac{dR_{gal}(\mu M_*, M_*)}{dM_{*1}dM_{*2}}$$

If we now use eq. (4.14) and eq. (4.18) we obtain

$$\frac{1}{M_*} \frac{dR_{gal}(M_*, \mu)}{dM_* d\mu} = \frac{1}{\mu M_*} \frac{dR_{gal}(\mu M_*, 1/\mu)}{dM_* d\mu}$$

hence the symmetry condition

$$\frac{dR_{gal}(M_*, \mu, z)}{dM_* d\mu} = \frac{1}{\mu} \frac{dR_{gal}(\mu M_*, 1/\mu, z)}{dM_* d\mu} \tag{4.20}$$

If we drop the superscripts and notice that M_* and μM_* can also be exchanged in the arguments of the two p_{occ} we can write the BH merger rate density as an integral over T only and get rid of the factor $1/2$

$$\frac{dR_{BH}}{dm_1 dm_2} = \iint_T p_{merg}(m_1, m_2, z) p_{occ}(m_1|M_*) p_{occ}(m_2|\mu M_*) \frac{dR_{gal}}{dM_* d\mu} dM_* d\mu \tag{4.21}$$

Do not forget that our goal is to shrink the integration area to make it coincide to that of the observed galactic merger rate eq. (4.2), and we still need a last step.
We call $U = \{[10^{9.7}\ M_\odot\ ,\ \infty) \times [0\ ,1]\}$ the integration region upon which the total observed merger rate density eq. (4.15) is evaluated and ask ourselves: can we further reduce the integration domain of eq. (4.21) from T to U?
We can cut the domain of integration for M_* due to the prior knownledge on $\Omega(f)$: (Ellis et al., 2023) and (Ellis et al., 2024a) showed that the signal is dominated by a few strong sources; moreover, the method presented in chapter 2 that we use to generate Monte Carlo evaluation of $\Omega(f)$ exploits this by generating only the signal given by the

strongest sources.
Inspecting the signal given by each source eq. (2.25) we see that the strongest signals are generated by both the closest and the heaviest SMBH binary pairs: we then find plausible to ignore the lightest SMBH mergers, since they will contribute only to the signal generated by weak sources $\bar{\Omega}_W$ and these sources barely change the modeled probability distribution of the signal;
If that is the case, it means that for our purposes there is some galactic mass below which the contribution of the galactic mergers to the SMBH merger rate density can be ignored. We decide to make the assumption that this threshold mass has the value of $10^{9.7}\ M_\odot$, in other words we assume that the observed merger rate eq. (4.15) contains all the information to correctly describe the SMBH merger rate density. As a rough estimate, eq. (2.6) tells us that we will consider all SMBH mergers in which the mass of the heaviest BH in a merging pair is above $\approx 13 \cdot 10^6\ M_\odot$. After these considerations, we are left with

$$\frac{dR_{BH}}{dm_1 dm_2} \approx p_{merg}(m_1, m_2, z) \iint_U p_{occ}(m_1|M_*) p_{occ}(m_2|\mu M_*) \frac{dR_{gal}}{dM_* d\mu} dM_* d\mu \ , \quad (4.22)$$

where, if we trace back to the beginning of this section, the differential galactic merger rate can be written as a function of the differential halo merger rate as

$$\frac{dR_{gal}}{dM_* d\mu} = M_* \frac{dR_{gal}(M_*, \mu M_*, z)}{dM_{*1} dM_{*2}} = \\ = M_* \cdot detJ(M_*, \mu M_*) \frac{dR_h(f^{-1}(M_*), f^{-1}(\mu M_*))}{dM_{h1} dM_{h2}} \ . \quad (4.23)$$

4.4 Using the observed rates

We have finally showed that the BH merger rate can be expressed as an integral over the same region of the (M_*, μ) plane on which we have the measure of $\Gamma_{tot}(z)$, but we still lack a way of writing the BH merger rate as a function of the total galactic merger rate. We could assume that the probabilities p_{occ} do not depend on the masses of the galaxies, but this is not how nature works, as it is widely known that a relation exists between galactic global properties and the central SMBH mass ((Cimatti et al., 2019), Section 5.4.4), so this is not a suitable solution. We need to find a smart way to write the integral eq. (4.22) so that $\Gamma_{tot}(z)$ appears. The idea here is to notice that we only have information regarding the overall redshift dependence of the merger rate density

while we lack information about its dependence on the mass of the galaxies. So we will keep the differential merger rate density provided by the EPS formalism while only changing its normalization: we define

$$\Gamma_{theo}(z) = \iint_U \frac{dR_{gal,EPS}(M_*, \mu)}{dM_* d\mu} dM_* d\mu \ . \tag{4.24}$$

The EPS function used here is obtained from eq. (4.23) and the differential halo merger rate density is the same as in (Ellis et al., 2023) and (Ellis et al., 2024a). We can look back at the plot in Fig. 3.1 and compare this theoretical total galactic merger rate density eq.(3.9) and its measured counterparts eq. (4.24): the measured merger rate is actually a bit smaller at low redshifts while it increases at high redshifts, and this could generate some differences later on, resulting in a smaller predicted GW signal which could increases p_{merg} to a higher value than the results of (Ellis et al., 2024a).
This change of normalization means that to obtain the differential BH merger rate density we evaluate

$$\frac{dR_{BH}}{dm_1 dm_2} \approx \Gamma_{tot}(z) \cdot \frac{1}{\Gamma_{theo}(z)} \iint_U p_{merg} p_{occ}(m_1|M_*) p_{occ}(m_2|\mu M_*) \frac{dR_{gal,EPS}}{dM_* d\mu} dM_* d\mu \ . \tag{4.25}$$

We recall the definition of the BH merger rate eq. (4.3) and all the cuts to the domain of integration that we made till eq. (4.22), so we can take all the steps back and say that

$$\frac{dR_{BH}}{dm_1 dm_2} \approx \frac{\Gamma_{tot}(z)}{2\Gamma_{theo}(z)} \cdot \iint_S p_{merg} p_{occ}(m_1|M_{*1}) p_{occ}(m_2|M_{*2}) \frac{dR_{gal,EPS}}{dM_{*1} dM_{*2}} dM_{*1} dM_{*2} \ . \tag{4.26}$$

4.5 The final BH merger rate

It can be useful to find a non-computationally expensive numerical evaluation of the integral eq. (4.26) to speed up the algorithm used to fit the data and that is exactly this section aim. If we substitute in it the definition of p_{occ} eq. (2.5), we get

$$\frac{dR_{BH}}{dm_1 dm_2} = k \iint_D exp\left\{ -\frac{1}{2\sigma^2} \left[ln^2\left(\frac{m_1}{\bar{m}_1}\right) + ln^2\left(\frac{m_2}{\bar{m}_2}\right) \right] \right\} \frac{dR_{gal,EPS}}{dM_{*1} dM_{*2}} dM_{*1} dM_{*2} \tag{4.27}$$

where

$$k = \frac{p_{merg}(m_1, m_2, z)\Gamma_{tot}(z)}{4\pi m_1 m_2 \sigma^2 \Gamma_{theo}(z)} \tag{4.28}$$

We recall that m_1 and m_2 are the masses of the merging SMBH and $\sigma = 1.1$. We do not make any assumption yet on the shape of p_{merg}, which could in theory could depend on both the SMBH masses and the redshift, so what follows is indipendent of this functional form.
We also recall that from eq. (2.6) the average masses of the merging SMBH $\bar{m}_i$ are a function of the merging galaxy masses M_{*i}

$$\bar{m}_i = 10^{8.95} \cdot \left(\frac{M_{*i}}{10^{11}\ M_\odot}\right)^{7/5}\ M_\odot \tag{4.29}$$

We can use this relation to define two new parameters

$$\alpha := \left(\frac{m_1}{10^{8.95}}\right)^{5/7} \times 10^{11}\ M_\odot\ ,\ \beta := \left(\frac{m_2}{10^{8.95}}\right)^{5/7} \times 10^{11}\ M_\odot \tag{4.30}$$

and substitute them in eq. (4.27) so that it becomes

$$\frac{dR_{BH}}{dm_1 dm_2} = k \iint_D exp\Bigg\{ -\frac{1.96}{2\sigma^2}\left[ln^2\left(\frac{M_{*1}}{\alpha}\right) + ln^2\left(\frac{M_{*2}}{\beta}\right)\right]\Bigg\} \frac{dR_{gal,EPS}}{dM_{*1}dM_{*2}} dM_{*1}dM_{*2} \tag{4.31}$$

We perform a change of variable to take the physical quantities out from the integral

$$x = ln\left(M_{*1}/\alpha\right) \implies dM_{*1} = \alpha e^x\, dx \tag{4.32}$$

$$y = ln(M_{*2}/\beta) \implies dM_{*2} = \beta e^y\, dy \tag{4.33}$$

so that it becomes

$$\frac{dR_{BH}}{dm_1 dm_2} = \alpha\beta k \iint_{\mathbb{R}^2} exp\left[-\frac{1.96}{2\sigma^2}(x^2+y^2) + x + y\right] \frac{dR_{gal,EPS}(\alpha e^x, \beta e^y)}{dM_{*1}dM_{*2}} dxdy \tag{4.34}$$

Now we focus on the argument of the exponential function in the integrand of this equation; we perform another variable change

$$a = \frac{1.4}{\sigma\sqrt{2}}x - \frac{\sigma\sqrt{2}}{2.8} \implies dx = \frac{\sigma\sqrt{2}}{1.4}da \tag{4.35}$$

$$b = \frac{1.4}{\sigma\sqrt{2}}y - \frac{\sigma\sqrt{2}}{2.8} \implies dy = \frac{\sigma\sqrt{2}}{1.4}db \tag{4.36}$$

that allows us to rewrite eq. (4.34) into

$$\frac{dR_{BH}}{dm_1 dm_2} = \frac{2\alpha\beta\sigma^2 k}{1.96} exp\left(\frac{\sigma^2}{1.96}\right) \iint_{\mathbb{R}^2} e^{-a^2-b^2} \frac{dR_{gal,EPS}}{dM_{*1}dM_{*2}}\left(\alpha e^{x(a)}, \beta e^{y(b)}\right) dadb \tag{4.37}$$

where

$$x = \frac{\sigma\sqrt{2}}{1.4}a + \frac{\sigma^2}{1.96} \ , \ y = \frac{\sigma\sqrt{2}}{1.4}b + \frac{\sigma^2}{1.96} \tag{4.38}$$

At the end, the differential BH merger rate is

$$\frac{dR_{BH}}{dm_1 dm_2} = \Gamma_{tot}(z)\frac{2\alpha\beta\sigma^2 k}{1.96} exp\left(\frac{\sigma^2}{1.96}\right) \iint_{\mathbb{R}^2} e^{-a^2-b^2} \frac{dR_{gal,EPS}}{dM_{*1}dM_{*2}}\left(\alpha e^{x(a)}, \beta e^{y(b)}\right) dadb \tag{4.39}$$

or, using the definition of the factor k eq. (4.28)

$$\frac{dR_{BH}}{dm_1 dm_2} = p_{merg}\frac{\Gamma_{tot}(z)}{\Gamma_{theo}(z)}\frac{\alpha\beta}{3.92\pi m_1 m_2} exp\left(\frac{\sigma^2}{1.96}\right) \times \\ \times \iint_{\mathbb{R}^2} e^{-a^2-b^2} \frac{dR_{gal,EPS}}{dM_{*1}dM_{*2}}\left(\alpha e^{x(a)}\beta e^{y(b)}\right) dadb \tag{4.40}$$

This is the final analytical expression of the SMBH merger rate density that we need.

5

Chapter 5: Numerical methods

5.1 Implementation of the model in the numerical code

This chapter contains details regarding a rewriting of the quantities presented in Chapter 2 but as were used in the code; moreover, it will contain a few remarks on the Python modules used. All quantities in this chapter are expressed into geometric units $c = G = 1$.

In the last chapter we showed that the SMBH merger rate density can be written as a function of the measured merger rate density $\Gamma_{tot}(z)$ and the theoretical differential galactic merger rate density predicted by the EPS formalism $dR_{gal,EPS}/dM_{*1}dM_{*2}$

$$\frac{dR_{BH}}{dm_1 dm_2} = p_{merg}\frac{\Gamma_{tot}(z)}{\Gamma_{theo}(z)}\frac{\alpha\beta}{3.92\pi m_1 m_2}exp\left(\frac{\sigma^2}{1.96}\right)\times \\ \times \iint_{\mathbb{R}^2} e^{-a^2-b^2}\frac{dR_{gal,EPS}}{dM_{*1}dM_{*2}}\left(\alpha e^{x(a)}\beta e^{y(b)}\right)dadb \quad (5.1)$$

Due to the particular form of the integrand, this integral can be evaluated in a really efficient way using the Gauss-Hermite quadrature: as explained in (Abramowitz & Stegun, 1965) an integral over all real numbers where a factor of the integrand is a Gaussian can be approximated by a sum of samples of the integrand over n points

$$\int_{-\infty}^{\infty} e^{-x^2} f(x)dx \approx \sum_{i=1}^{n} w_i f(x_i) \quad (5.2)$$

with weights

$$w_i = \frac{2^{n-1}n!\sqrt{\pi}}{n^2\left[H_{n-1}(x_i)\right]^2} \quad (5.3)$$

and the x_i are the roots of the Hermite polynomial $H_{n-1}(x)$. We chose $n = 3$, so that

$$x_i = \left(0, \sqrt{\frac{3}{2}}, -\sqrt{\frac{3}{2}}\right) \quad , \quad w_i = \left(\frac{2}{3}\sqrt{\pi}, \frac{\sqrt{\pi}}{6}, \frac{\sqrt{\pi}}{6}\right) \quad (5.4)$$

We must keep in mind that in our case these values must be applied to a and b, so we substitute these values of x_i into eq. (4.38) and instead call

$$x_i = \left(exp\left(\frac{1.21}{1.96}\right), exp\left(\frac{1.21}{1.96} + \frac{\sigma\sqrt{3}}{1.4}\right), exp\left(\frac{1.21}{1.96} - \frac{\sigma\sqrt{3}}{1.4}\right)\right) \tag{5.5}$$

so that the BH merger rate is evaluated using

$$\frac{dR_{BH}}{dm_1 dm_2} = p_{merg}(m_1, m_2, z)\Gamma_{tot}(z) \cdot A(m_1, m_2, z) \tag{5.6}$$

where the function $A(m_1, m_2, z)$ is

$$A(m_1, m_2, z) = \frac{0.47}{\pi \cdot \Gamma_{theo}(z)} \frac{\alpha\beta}{m_1 m_2} \sum_{i=1}^{3}\sum_{j=1}^{3} \frac{dR_{gal,EPS}}{dM_{*1} dM_{*2}} (\alpha \cdot x_i, \beta \cdot x_j) \tag{5.7}$$

This is the actual function used in the code to evaluate the SMBH differential merger rate density, saving a lot of time by estimating an integral using only 9 values of its integrand function. The halo mass function used for evaluating the EPS formalism as in (Ellis et al., 2023) and (Ellis et al., 2024a) was calculated using the same code as in (Bird et al., 2013), but with the Press-Schechter halo mass function instead of the Sheth-Tormen. The probability per unit time that two halo merger was evaluated as in (Ellis et al., 2023) and (Erickcek et al., 2006).
The average number of sources eq. (2.23) can be rewritten using eq. (2.2), eq. (2.18), eq. (2.20) and eq. (2.21)

$$\begin{aligned}\bar{N}(f_i) = \iint_{f\in[f_i, f_{i+1}]} d\vec{\lambda} d\tau = \iint_{\ln f\in[\ln f_i, \ln f_{i+1}]} \left|\frac{dt}{d\ln f}\right| d\vec{\lambda} d\ln f = \\ = \frac{5}{96} \iiiint_W \frac{g(\mathcal{M}_c, f, z)}{\mathcal{M}_c^{5/3}(\pi f)^{8/3}(1+z)^{11/3}} \frac{dR_{BH}}{d\mathcal{M}_c d\eta} \frac{dV_c}{dz} dz d\eta d\mathcal{M}_c d\ln f\end{aligned} \tag{5.8}$$

where the function g has in it the information about the environmental effects

$$g(\mathcal{M}_c, f, z) = \left(1 + \left(\left(\frac{\mathcal{M}_c}{10^9\ M_\odot}\right)^{0.4} \frac{f(1+z)}{f_{ref}}\right)^{-\alpha_{PW}}\right)^{-1} \tag{5.9}$$

and the region of integration is

$$W = \{\{z \in [0,3]\} \times \{\eta \in [0\ , 1/4]\} \times \{\mathcal{M}_c \in [\mathcal{M}_{c,min}\ , \mathcal{M}_{c,max}]\} \times \{\ln f \in [\ln f_i\ , \ln f_{i+1}]\}\} \tag{5.10}$$

We have chosen to put some limits on the values of the possible $\mathcal{M}_c$ due to both efficiency and stability. There are multiple integrals which involve integration of the BH merger

rate (2.11) over the chirp mass, and this function does not have a cut-off for low values of BH mass, so we have to choose a lower boundary, $\mathcal{M}_{c,min}$. We are interested in generating a signal caused by SMBH merger only so we could assume that the minimum chirp mass has the value for which both BHs involved in the merger have the smallest mass possible of $10^5\ M_\odot$ to be considered SMBH; this seems to be a rather arbitrary choice, but fortunately for this lower limit the important thing is not the choice of the value itself but rather the consistent use of it in the code: every integral over chirp masses must have the same minimum chirp mass. We made the program run for other values of $\mathcal{M}_{c,min}$ and the results do not depend on it as long as this change is applied to all integrals which involves integration along the chirp mass $\mathcal{M}_c$. The upper value was chosen as $\approx 10^{13}\ M_\odot$, so that it was slightly above the cut-off mass of the BH merger rate evaluated with the EPS formalism at $z = 0$.
The integral eq. (2.23) was numerically evaluated with the Gaussian quadrature with 5 points as in (Abramowitz & Stegun, 1965); this is true for all the other integrals of this section unless it is said otherwise.
We can also rewrite the probability of finding a single source for a given signal strength eq. (2.24) using the property of the Dirac delta to eliminate the dependence on the chirp mass inside the integral

$$\delta(f(x)) = \frac{\delta(x - x_0)}{|f'(x_0)|} \quad where \quad f(x_0) = 0 \tag{5.11}$$

yielding

$$P^{(1)}(\Omega|f,\vec{\theta}_M) = \frac{1}{\mathcal{N}} \int_0^3 dz \int_0^{1/4} d\eta \frac{\Omega^{-6/5} g(\mathcal{M}_{c,o}, f, z)}{64(\pi f)^2 (1+z)^3} \left(\frac{5\pi d_L^2 \rho_c}{8(1+z)}\right)^{-1/5} \frac{dV_c}{dz} \frac{dR_{BH}}{d\mathcal{M}_c d\eta}(\mathcal{M}_{c,o}, \eta) \tag{5.12}$$

where $\mathcal{M}_{c,o}$ is just the chirp mass

$$\mathcal{M}_{c,o} = \frac{1}{\pi f(1+z)} \left(\frac{5\pi \rho_c d_L^2}{8(1+z)} \Omega\right)^{3/10} \tag{5.13}$$

The factor outside of the integral $\mathcal{N}$ is just a normalization factor for the probability

$$\mathcal{N} = \iiint_X \frac{5 d_L^2 \rho_c \cdot g(\mathcal{M}_{c,o}, f, z)}{512\pi f^2 (1+z)^4} \left(\frac{5\pi d_L^2 \rho_c}{8(1+z)} \Omega\right)^{-6/5} \frac{dV_c}{dz} \frac{dR_{BH}}{d\mathcal{M}_c d\eta}(\mathcal{M}_{c,o}, \eta) dz d\eta d\Omega \tag{5.14}$$

Its integration domain is

$$X = \{\{z \in [0,3]\} \times \{\eta \in [0\ ,1/4]\} \times \{\Omega \in [\Omega_{min}\ ,\Omega_{max}]\}\}\ . \tag{5.15}$$

The choice of limits of integration for the signal Ω is the same as for the chirp mass: the values were fixed by using the chirp mass eq. (5.13) with $z = 0.1$ for the maximum signal and $z = 3$ for the minimum; fortunately the maximum signal corresponds to a mass well above the cut-off of the BH merger rate so the redshift choice does not impact it. The frequency used is the central frequency of the bin. Once this probability was created in each bin, it was fit with `scipy.interpolate.cubicspline` (d. Boor, 1978) to make the generation of signals much faster.
We then chose the number of strong signals $\bar{N}_s = 500$ because, as explained in the appendix of (Ellis et al., 2024a), this allow us to ignore the contribution of all the others weak sources, so we can put $\bar{\Omega}_W \approx 0$. With this in mind, we searched for Ω_{th} by finding the zero of the function

$$Z(\Omega) = \log_{10}(\bar{N}_s) - \log_{10}(\bar{N}) - \log_{10}\left(\int_{\Omega}^{\Omega_{max}} P^{(1)}(\Omega')d\Omega'\right) \tag{5.16}$$

the zero was searched with the function `brentq` (Brent, 1973) implemented in `scipy.optimize`, with a tolerance `xtol`$= 0.001$. Following this we generated the strong signals: we extracted 4×10^4 times 500 random number each with `numpy`, then we built the cumulative inverse function of the fit probability distribution and finally transformed the random distribution into the target one with the Inverse Transform Sampling (Devroye, 1986). In each one of the 4×10^4 extraction we summed the 500 strong signals and divided the sum by the bin frequencies as in eq. (2.27) to obtain 4×10^4 samples of the signal. For each one of the distribution of signals we then used the Kernel Density Estimation method (implemented in Python by the module `KDE.py` (Odland, 2018) to convert the histogram of the distribution of these strong signals into its continuous probability distribution. In particular, the function used was `FFTKDE`, with the Epanechnikov Kernel and the bandwitdh was selected with the Improved Sheather Jones (ISJ) method.
The threshold between the generated distribution and the approximation for strong signals detected eq. (2.31) was set for each bin as the maximum Ω of the generated KDE: above it, the distribution was approximated with the said equation.
We used the same likelihood as in (Ellis et al., 2024a), which means eq. (2.40), and we found its maximum by searching for the minimum of $-\ln\mathcal{L}$: first, we performed a coarse grid search to identify a good starting point (Press et al., 2007), and then we refined the solution using the Nelder–Mead method (Press et al., 2007), implemented in the Python module `scipy.optimize.minimize` (Gao & Han, 2012).

6

Chapter 6: Results and conclusions

6.1 Results

We will now present the results and the conclusions of this thesis. We choose to perform two different analysis based on the data: one in which we used all the same NANOGrav bins with $f < 30\ nHz$ as in (Ellis et al., 2024a), and another one in which we ignored the data from bin 8, since it seems that a strong source is the main signal, overcoming the noise of the SGWB (Agazie et al., 2023), (Ellis et al., 2024a).

6.1.1 Fit to all NANOGrav bins

The best fit values for both the GW only and GW+environment models can be found in table (6.1), while their likelihoods can be seen in fig. 6.1; starting with the GW only model, its the main result is that the SMBH merger probability is $p_{merg} = 1.45^{+0.34}_{-0.51}$ seems to be bigger than 100 %, while being still within margin of error compatible with it. This is a direct consequence of the difference between the merger rate density used, as it is smaller than the EPS one at low redshifts, thus generating a smaller signal from strong sources, hence requiring a higher BH merger efficiency to fit the data. As in (Ellis et al., 2024a), the only problem for this model is a difficulty in fitting the bin 1, as can be seen in fig. 6.1; removing this bin from the data further increases the value of p_{merg}. Moreover there is no reason to remove it from the data so we keep it and confirm that also our model does not perform well for $f \in [1.98\ nHz, 3.96\ nHz]$. Nevertheless, since $p_{merg} = 1.45^{+0.34}_{-0.51}$, this model tells us that SMBH alone could not be the only source of the signal, suggesting the presence of at least another one of the cosmological sources listed in the introduction (Chapter 1) to account for $\approx 50\%$ of the observed signal. Another possibility is that the merger rate density used in this work is an underestimation of the real value, which leads to overestimating p_{merg}.
Moving on to the next model, the likelihood for the GW+environment model was first explored with the Python module `emcee` (Foreman-Mackey et al., 2013) assuming that $p_{merg} \in [0, 1]$, $\alpha_{PW} \in [0, 6]$ and $\log_{10} f_{ref} \in [-10, -7]$. In this second case, the results can be seen in fig. 6.2. This plot was created with a sample of roughly 28 thousand

points; this is probably too low number of samples to determine the exact shape of the contour plot, but it required a really long time to be created: due to the low efficiency of this method, this is the only contour plot for the likelihoods of the models. Nevertheless, it still provides us with interesting information regarding the behaviour of the likelihood for GW+environment models:

- high values of p_{merg} are strongly favoured;
- the likelihood has a strong peak for $-\log_{10} f_{ref}$ values between $\sim 8 - 8.2$
- the distribution of the power-law index α_{PW} linking the GW and environmental timescales is not fully resolved; the following evaluations of the likelihood shown in this chapter confirm that the exact value of α_{PW} is not that important of the model, since it can span a wide range of parameters.

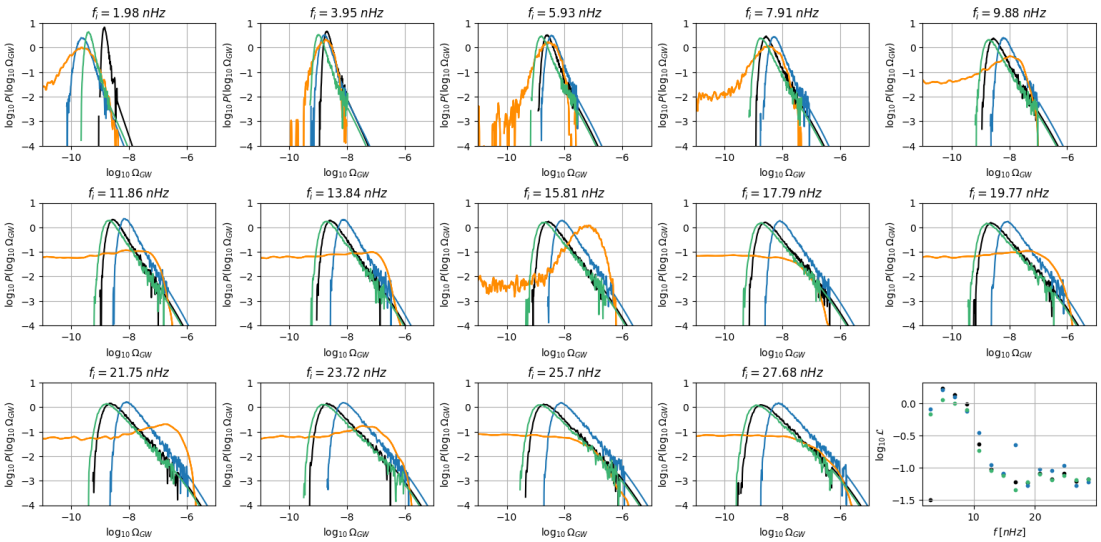

Figure 6.1. Comparison among the NANOGrav data (orange), the GW only model (black), the limited GW+environment model (green) and the free GW+environment model (blue) modeled over all NANOGrav bins. In the bottom right we also show the logarithm of the likelihood function in each bin, each model having the mentioned color.

All things considered, the exact value of α_{PW} does not seem to be important, as in (Ellis et al., 2024a), while p_{merg} and f_{ref} seem to be the important parameters of the model. There is a reason why our α_{PW} and f_{ref} are higher than those found in (Ellis et al., 2024a), and one can see that from reasoning on their effect on the GW-only model: α_{PW} changes the tilt of the fit SGWB for frequencies smaller than $\sim f_{ref}$. Now, since our GW-only model fit badly only bin 1, the introduction of the environmental

effects is actively trying to improve the fit mainly for this bin, rather than the 3-4 that needed improvement in (Ellis et al., 2024a), hence requiring a higher α_{PW} (increasing the tilt) for lower frequencies. This can be seen from the differences in the likelihoods of bin 1 of fig. 6.3.

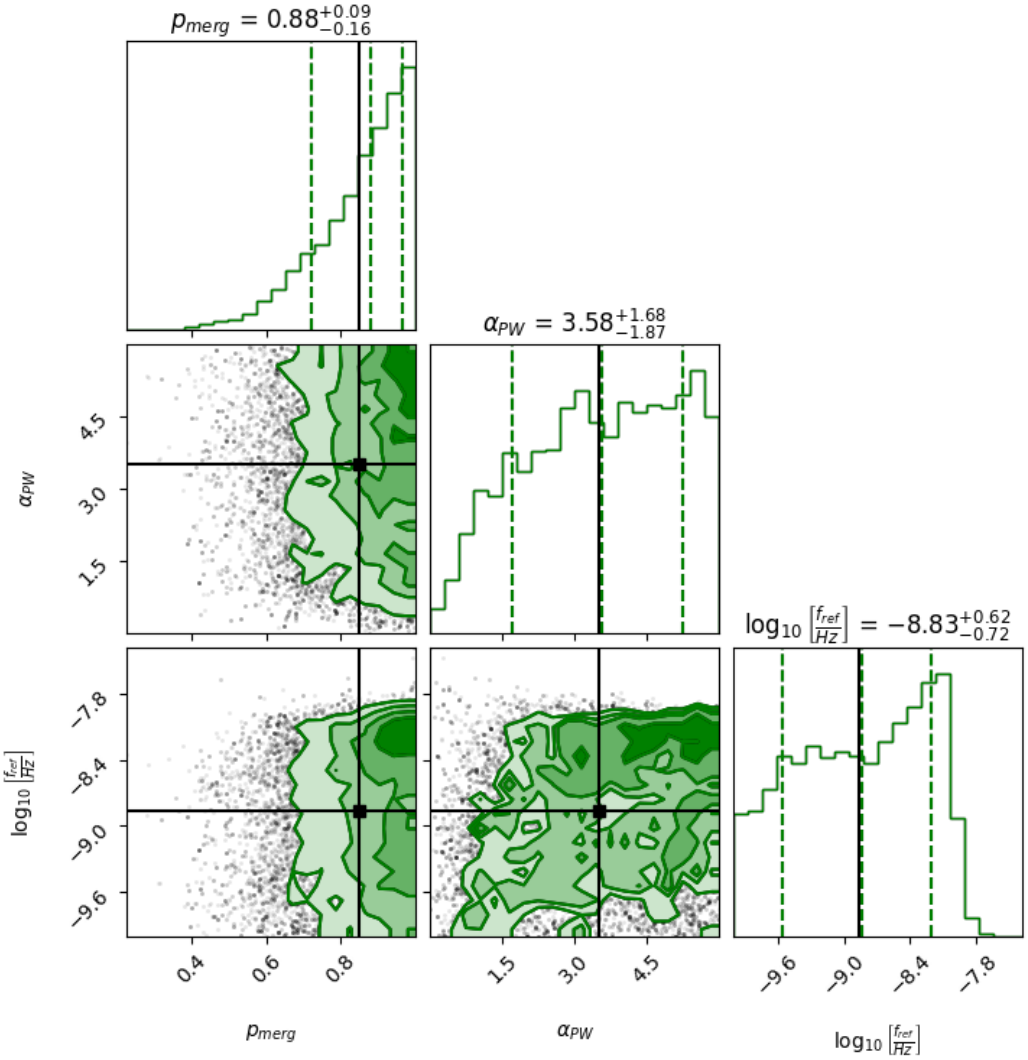

Figure 6.2. Plot of the contour levels of the posterior probability for the parameters of the GW+environment model with limited uniform prior.

The histogram for p_{merg} only in fig. 6.2 and the previous result for the GW only model both suggest us to remove the said prior to explore the possibility of values of p_{merg} bigger than 1, i.e. that we are underestimating the signal; we then again searched for

the maximum of the likelihood, and again the results are shown in table (6.1). As for the GW only model case, it is again suggested that SMBH merging could be the cause of just a fraction of the signal observed by NANOGrav, around a third for this case: if that is true, both best fit values for α_{PW} and $\log_{10} f_{ref}$ should not be taken as the exact values due to the possible contamination in the signal of additional cosmological sources. As for the GW only model, the possibility of having worked with an underestimation of the total merger rate density is still on the table. We also want to underline the likelihood plot in fig. 6.1, and in particular that all 3 models seem to better reproduce the first 4 bins rather than the other by nearly an order of magnitude, with the said exception for bin 1 for the GW only model. The likelihood ratio eq. (2.41) can be easily evaluated for the models, and correspond to $\lambda = 2(\ln \mathcal{L}_{high} - \ln \mathcal{L}_{low}) = 10.24$ for the GW only and free GW+environment model, and $\lambda = 2.68$ for the GW only and the limited GW+environment model; as the likelihood ratio test (Casella & Berger, 2002) says, both of these values must be confronted with the χ^2 distribution with two degrees of freedom, giving as a result that the free GW+environment model model is favoured at a 2.5σ Confidence Level (CL), but the limited GW+environment model is not favoured enough relative to the GW only model. This means that if SMBH are the only source of the SGWB, the environmental effects are not significative enough to disfavour the GW only model, but at the same time the strong increase in the likelihood for the third model means that the environmental effects are definetely there; more importantly, the data suggests that SMBH alone are not the only source of the SGWB since $p_{merg} > 100\%$: this possibly hints that one or more of the many cosmological processes for generating a SGWB could be put on the table to explain this strong discrepancy (SMBH seem to account for just ~ 30 % of the signal). Another possibility for the high value measured for p_{merg} could be in the uncertainties on $p_{occ}(m|M, z)$, since $\bar{m}$ seems to increase not only with M_*, but also with z (Cimatti et al., 2019), (Nipoti, 2025). Sources with higher masses will generate a stronger signal, hence decreasing p_{merg}: this effect clearly depends on how $\bar{m}$ changes with z relative to $1/d_L^2(z)$ and dV_c/dz, but this relation is still poorly observationally constrained. Regardless, one should still be advised with the index α_{PW} and the frequency f_{ref} since most of the SGWB seems to be generated by cosmological sources, making it extremely pollutted and difficult to recover the real behaviour of the circumbinary gas and/or loss cone dynamics. It is also worthy to notice that we assumed an istantaneous emission between pairs of SMBH once the galaxies has merged, ignoring the time needed for both SMBH to reach the core of the newly formed galaxies: if one also included this delay, the signals would be generated at a smaller z, making them stronger and hence requiring a smaller p_{merg}, but this inclusion could

Frequency Bins	Model	p_{merg}	α_{PW}	$\log_{10}[f_{ref}/Hz]$	$\log \mathcal{L}$
All bins	GW only	$1.45^{+0.34}_{-0.51}$	–	–	-27.84
	GW+environment, limited	$1.00^{+0.00*}_{-0.11}$	$5.30^{+22.57*}_{-2.68}$	$-8.08^{+0.11}_{-0.24}$	-26.34
	GW+environment, free	$3.40^{+1.30}_{-0.18*}$	$6.50^{+0.05*}_{-2.95}$	$-7.84^{+0.00*}_{-0.05}$	-22.72
All but bin 8	GW only	$1.10^{+0.53}_{-0.33}$	–	–	-24.83
	GW+environment, limited	$1.00^{+0.00*}_{-0.12}$	$6.76^{+148.00}_{-4.21}$	$-8.09^{+0.12}_{-0.22}$	-23.20
	GW+environment, free	$2.50^{+1.13}_{-0.46}$	$5.71^{+0.96*}_{-2.70}$	$-7.87^{+0.06}_{-0.07}$	-21.21

Table 6.1. This table contains all the parameters that maximize the likelihood for each model. The errors are computed for each parameter individually with the delta log likelihood method (Casella & Berger, 2002). The errors indicated with * were not obtained as the other, but are the limits beyond which the model does not work anymore.

also predict an even steeper α_{PW}. All 3 models seem to poorly fit the high frequency bins, but this is probably due to the difference in the shape between the probabilities of our model, artificially cut at $\Omega > \Omega_{th}$, and the NANOGrav violins: the violins at these frequencies are much less peaked than the violins in the first bins. Changing model also does not seem to increase significantly the likelihood in this is part, even if the difference between the most probable signal sampled changes by one order of magnitude between models with and without environmental effects.

6.1.2 Fit to all NANOGrav bins except bin 8

In all the cases presented in the previous section we focused on the possible issues between models and bin 1, but there could be also an issue with the data, bin 8 ($f_i = 15.81\ nHz$). We can see in the fig. 6.1 that the best fit without limits is bought up by bin 8 (look at the likelihood plot in each bin): in fact, both (Agazie et al., 2023) and (Ellis et al., 2024a) suggested the possibility of a contamination of the SGWB by an individual strong source, as the KDE of the data is higher than expected relative to the close bins and the best fit power laws proposed in literature. If that is the case, the signal of the SWGB submerged in the noise and this bin should be ignored, so we decided to repeat the best fit of the three said model without the data of bin 8.

The best fit values for the GW only, the limited GW+environmental and the free GW+environmental model are again listed in table (6.1) and shown in fig. 6.3: in the figure, the models for bin 8 were plotted even if it was not used for the evaluation of the likelihoods.

We start by noticing that the removal of bin 8 makes the GW only model much more compatible with the assumption that the signal is generated by SMBH only, but as can be seen from the likelihood plot, the bin 1 has the same issue of being bad fit as before. For the GW only model and the free GW+environmental model $\lambda = 7.24$, reducing the significativity at a 1.9σ CL, while for the GW only and the limited GW+environmental model $\lambda = 3.26$, again having too weak statistical significance. The removal of bin 8 still keeps the possibility of the presence of other cosmological sources statistically significant while being slightly smaller: this is because in this case neither the GW only model nor the free GW+environment model are trying to fit bin 8 (look at their difference in likelihoods in fig. 6.1), the main difference for the models still being in bin 1.

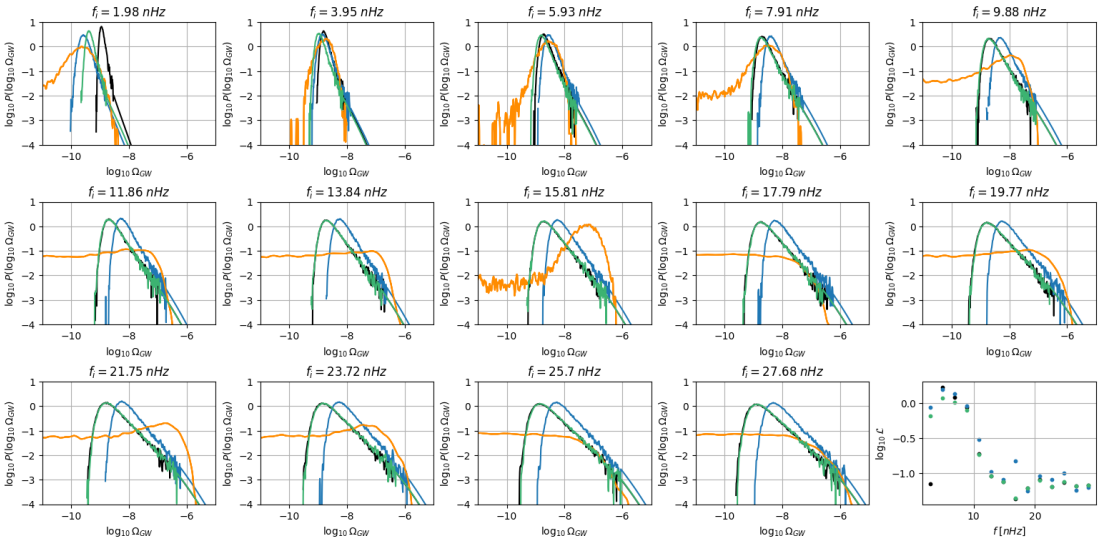

Figure 6.3. Comparison among the NANOGrav data (orange), the GW only model (black), the limited GW+environment model (green) and the free GW+environment model (blue) modeled over all NANOGrav bins except for bin 8. In the bottom right we also show the logarithm of the likelihood function in each bin, each model having the mentioned color. Bin 8 ($f_i = 15.81\ nHz$) is represented here for comparison, but was not used for determining the likelihoods

6.1.3 On the nature of the strong source in bin 8

It is possible to use the data in our possession to find a crude relation to help with the identification of the source in bin 8: first of all, one need to identify the source's signal, and that is done by subtracting the average value of the probability distribution of NANOGrav's bin 8 data to the value of Ω for which the likelihood in bin 8 is maximum for the last model in table (6.1); the excess noise seems to be generated by a source with $\bar{\Omega}_{data} - \Omega_{model} = \Omega_8 \approx (6.88 \pm 2.84) \times 10^{-8}$. Then, one could rewrite eq. (2.25), taking as $f = 16.80\ nHz$ the central frequency of bin 8, to find that this merger should have a $\mathcal{M}_c$ and should be living at a z such that

$$\left[\frac{\mathcal{M}_c}{10^6\ M_\odot}\right]\left[(1+z)^{13/10}\left[\frac{d_L(z)}{Mpc}\right]^{-3/5}\right] \approx 1855 \pm 495\ . \tag{6.1}$$

This relation is plot in fig. 6.4. In the "local" case $z = 0$ the relationship is the same, but with the standard distance d instead of the luminosity distance d_L. The local case could also be used to verify that this source is not placed in the center of the Milky Way, since to generate the observed signal from a distance of $\approx 8\ kpc$ (Genzel et al., 2010) we should need a source with a chirp mass $\approx 9.17 \cdot 10^7\ M_\odot$, much bigger than anything that could be obtained with the single SMBH observed having a mass of $4.4 \times 10^6\ M_\odot$ (Genzel et al., 2010).

Rather than searching for the SMBH, one could be more interested in finding the newly formed galaxy: for that, one just need the SMBH-galactic mass relation eq. (2.6), then call $M_* = M_{*,1} + M_{*,2}$ the stellar mass of the host galaxy and recall the mass ratio μ of the galaxies (and of the SMBH pair) to find

$$\left[\frac{M_*}{10^{11}\ M_\odot}\right] \approx (1.74 \pm 0.46)\frac{(1+\mu)(1+\mu^{7/5})^{1/7}}{\mu^{3/5}(1+z)^{13/10}}\left[\frac{d_L(z)}{Mpc}\right]^{3/5}\ . \tag{6.2}$$

This relation is plot in fig. 6.4. The expected mass of the host galaxy is also really high, meaning that there is a possibility that there is not just one strong source in bin 8, but possibly 2 or more. Nevertheless, one should expect to find the source of bin 8 in a galaxy result of a major merger, since it requires a lower mass for the host. The dependence on the redshift makes possible that the source is not necessarely in the local Universe but also at a high-redshift; unfortunately massive galaxies were rarer in the early Universe so it is still more probable that the source is somewhere in our vicinity. Another problem regarding a possible high redshift source is that for these high masses it could not have had time to grow to these big masses needed for the signal. This relationship could also break down for high redshifts, since the used SMBH-galaxy mass

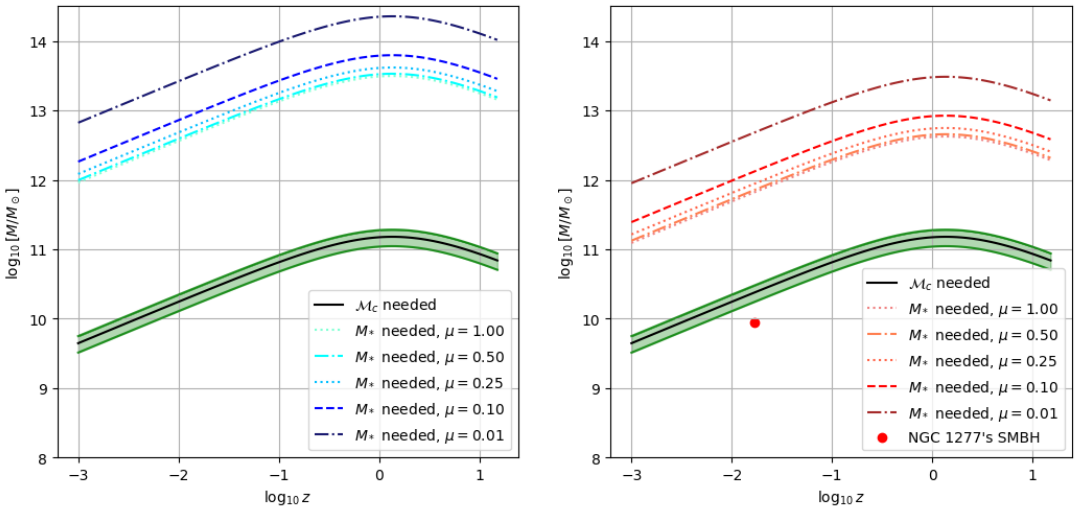

Figure 6.4. This figure shows the chirp mass eq. (6.1), with its 1σ CL in green, that a SMBH pair should have in order to produce the excess signal detected in bin 8. We also plotted the expected mass of the galaxy as a function of the redshift and the mass ratio, both with the usual SMBH-galaxy mass ratio eq. (2.6), and both with a 10 times higher ratio. The red dot is the expected $\mathcal{M}_c$ for the detected central dark mass in NGC 1277 if both SMBH have half of the detected mass

relation was found in the local Universe, while it is believed that in the early Universe the ratio between SMBH mass and their host mass was higher (Cimatti et al., 2019), (Nipoti, 2025). With this in mind, we also re-evaluated the expected mass of the host galaxy eq. (6.2) in the case in which the SMBH-galaxy mass ratio was 10 times the local one eq. (2.6), as should be for the case of high z galaxies or relic galaxies (Nipoti, 2025):

$$\left[\frac{M_*}{10^{10}\ M_\odot}\right] \approx (2.34 \pm 0.62)\frac{(1+\mu)(1+\mu^{7/5})^{1/7}}{\mu^{3/5}(1+z)^{13/10}}\left[\frac{d_L(z)}{Mpc}\right]^{3/5} . \tag{6.3}$$

This relation is plot in fig. 6.4. Lower mass galaxies are much less rare than high mass galaxies due to the power-law nature of the galaxy density function (Mortlock et al., 2015), but it still may be difficult to find the host galaxy due to the rarity of galaxies with a SMBH-stellar mass ratio $10\times$ the average one. As a reference, we also plot one case of close relic galaxy, NGC 1277: this galaxy has a redshift $z = 0.017$, and measures based on CO(1-0) emission suggest that it has a central SMBH with a mass $M \sim 2 \cdot 10^{10} M_\odot$ (Scharwächter et al., 2016): if we assume that the unknown central mass is divided into two SMBH with the same mass, we could estimate both its $\mathcal{M}_c$, almost placing the relic along eq. (6.3) (see fig. 6.4). A really ancient merger

generating the galaxy would have brought this hypothetical SMBH binary to the center of NGC 1277; if we look at the timescale this is still plausible: both SMBH had all the time to reach the center of the new galaxy but not the time to merge yet: we can evaluates t_{GW} for the expected $\mathcal{M}_c = 8.71 \cdot 10^9\ M_\odot$ and for the central frequency of bin 8 $f = 16.80\ nHz$, and find $t_{GW} = 4\tau \approx 78\ Gyr \gg t_H$, meaning that such a binary did not have enough time to merge; moreover, from the best-fit values for α_{PW} and f_{ref} in the case without bin 8, one can estimate $t_{env} \approx 4319\ Gyr$, a strong increase as one should expect. Using other best fit parameters does not change this result. Unfortunately, there are two problems with this scenario:

- even this extremely massive dark mass could not be enough to fill the signal gap alone, since NGC 1277 lives below eq.(6.1): it may be that another one strong source is present in bin 8. Moreover, the used $\mathcal{M}_c$ could be an overestimation of the real value since other measures from the same paper are more in agreement with a mass range $5 \cdot 10^9 - 1.7 \cdot 10^{10}\ M_\odot$;
- a consequent merger with another lighter galaxy could have shrunk down the orbit of the binary SMBH, strongly decreasing both timescales (see Chapter 1).

Nevertheless, all of this subsection can be used as a guideline for detecting the source(s) that generate the excess signal of bin 8.

6.2 Conclusions

In this thesis we studied the possibility that the observed SGWB is generated by merging SMBHs, in particular we implemented a method for the evaluation and use of the observed galactic merger rate to obtain a model for the SGWB. We tested both a model for the merging of SMBH driven by GW emission only, and a model with additional environmental effect for the energy loss of the binary SMBHs. The main conclusions of this thesis are the following:

1. The merger rate density measured for galaxies with a mass larger than $\sim 5 \cdot 10^9\ M_\odot$ is $\Gamma_{tot}(z) = 6.03(1+z)^{5.5} \exp(-1.5z)\ Mpc^{-3}\ Gyr^{-1}$; it seems to be in agreement or slightly lower than the rate expected in literature by the EPS model at low redshifts, while being significantly higher than the EPS prediction at higher redshift (see in fig. 3.1).
2. Galactic merger rate density seems to suggest that the SGWB has a hybrid origin, both being generated by the astrophysical process and at least one other cosmological process, the latter generating ≈ 70 % of it. The presence of environmental

effects is confirmed but it is not clear, since it is partially hidden behind the pollution generated by cosmological sources. Nevertheless, both due to theoretical and observational uncertainties, the result is indicative and should be investigated more.

3. The possibility of a source in bin 8, as described in literature, is considered by repeting the fit without it; the model without environmental effects becomes much better, with a p_{merg} in agreement with the possibility that the signal is generated by astrophysical sources only. Nevertheless the introduction of environmental effects seems to confirm that at least one cosmological source is needed to better fit the NANOGrav data. A criterion for the selection of a possible host for bin 8 source is also given, needing a high chirp mass $\approx 10^{10} - 10^{11}\ M_{\odot}$ for a possible source in this bin, either inhabiting a very massive low z galaxy or a relic galaxy, such as NGC 1277. There is also the possibility that more than one source generate the excess signal in bin 8.

Bibliography

Abramowitz, M., & Stegun, I. A. 1965, Handbook of mathematical functions with formulas, graphs, and mathematical tables

Agazie, G., Anumarlapudi, A., Archibald, A. M., et al. 2023, ApJ, 951, L8, doi: 10.3847/2041-8213/acdac6

Begelman, M. C., Blandford, R. D., & Rees, M. J. 1980, Nature, 287, 307, doi: 10.1038/287307a0

Binney, J., & Tremaine, S. 1987, Galactic Dynamics (Princeton Series in Astrophysics)

Bird, S., Vogelsberger, M., Sijacki, D., et al. 2013, MNRAS, 429, 3341, doi: 10.1093/mnras/sts590

Brent, R. P. 1973, Algorithms for Minimization without Derivatives, 1st edn. (Englewood Cliffs, New Jersey: Prentice-Hall)

Carroll, S. M., Press, W. H., & Turner, E. L. 1992, ARA&A, 30, 499, doi: 10.1146/annurev.aa.30.090192.002435

Casella, G., & Berger, R. L. 2002, Statistical inference, Vol. 2 (Duxbury Pacific Grove, CA)

Cimatti, A., Fraternali, F., & Nipoti, C. 2019, Introduction to Galaxy Formation and Evolution: From Primordial Gas to Present-Day Galaxies

Conselice, C. J., Mundy, C. J., Ferreira, L., & Duncan, K. 2022, ApJ, 940, 168, doi: 10.3847/1538-4357/ac9b1a

d. Boor, C. 1978, A Practical Guide to Splines (New York: Springer Verlag)

Devroye, L. 1986, Non-Uniform Random Variate Generation(originally published with (Springer-Verlag). http://cg.scs.carleton.ca/~luc/rnbookindex.html

Duncan, K., Conselice, C. J., Mundy, C., et al. 2019, ApJ, 876, 110, doi: 10.3847/1538-4357/ab148a

Eisenstein, D. J., & Hu, W. 1998, ApJ, 496, 605, doi: 10.1086/305424

Ellis, J., Fairbairn, M., Hütsi, G., & et al. 2023, A&A, 676, A38, doi: 10.1051/0004-6361/202346268

Ellis, J., Fairbairn, M., Hütsi, G., et al. 2024a, Phys. Rev. D, 109, L021302, doi: 10.1103/PhysRevD.109.L021302

Ellis, J., Fairbairn, M., Franciolini, G., et al. 2024b, Phys. Rev. D, 109, 023522, doi: 10.1103/PhysRevD.109.023522

EPTA Collaboration, Antoniadis, J., Babak, S., et al. 2023, A&A, 678, A48, doi: 10.1051/0004-6361/202346841

Erickcek, A. L., Kamionkowski, M., & Benson, A. J. 2006, MNRAS, 371, 1992, doi: 10.1111/j.1365-2966.2006.10838.x

Foreman-Mackey, D., Hogg, D. W., Lang, D., & Goodman, J. 2013, PASP, 125, 306, doi: 10.1086/670067

Gao, F., & Han, L. 2012, Comput. Optim. Appl., 51, 259, doi: 10.1007/s10589-010-9329-3

Genzel, R., Eisenhauer, F., & Gillessen, S. 2010, Reviews of Modern Physics, 82, 3121, doi: 10.1103/RevModPhys.82.3121

Girelli, G., Pozzetti, L., Bolzonella, M., et al. 2020, A&A, 634, A135, doi: 10.1051/0004-6361/201936329

Hellings, R. W., & Downs, G. S. 1983, ApJ, 265, L39, doi: 10.1086/183954

Hoffman, L., & Loeb, A. 2007, MNRAS, 377, 957, doi: 10.1111/j.1365-2966.2007.11694.x

Lacey, C., & Cole, S. 1993, MNRAS, 262, 627, doi: 10.1093/mnras/262.3.627

Merritt, D. 2013, Classical and Quantum Gravity, 30, 244005, doi: 10.1088/0264-9381/30/24/244005

Merritt, D., Alexander, T., Mikkola, S., & Will, C. M. 2011, Phys. Rev. D, 84, 044024, doi: 10.1103/PhysRevD.84.044024

Moody, M. S. L., Shi, J.-M., & Stone, J. M. 2019, ApJ, 875, 66, doi: 10.3847/1538-4357/ab09ee

Mortlock, A., Conselice, C. J., Hartley, W. G., et al. 2015, MNRAS, 447, 2, doi: 10.1093/mnras/stu2403

Muñoz, D. J., Miranda, R., & Lai, D. 2019, ApJ, 871, 84, doi: 10.3847/1538-4357/aaf867

Nipoti, C. 2025, A&A, 697, A74, doi: 10.1051/0004-6361/202553930

Odland, T. 2018, doi: 10.5281/zenodo.2392268

Pearson, W. J., Wang, L., Alpaslan, M., et al. 2019, A&A, 631, A51, doi: 10.1051/0004-6361/201936337

Peters, P. C., & Mathews, J. 1963, Physical Review, 131, 435, doi: 10.1103/PhysRev.131.435

Phinney, E. S. 2001, arXiv e-prints, astro, doi: 10.48550/arXiv.astro-ph/0108028

Press, W. H., Teukolsky, S. A., Vetterling, W. T., & Flannery, B. P. 2007, Numerical Recipes: The Art of Scientific Computing (Third Edition) (Cambridge University Press)

Reines, A. E., & Volonteri, M. 2015, ApJ, 813, 82, doi: 10.1088/0004-637X/813/2/82

Scharwächter, J., Combes, F., Salomé, P., Sun, M., & Krips, M. 2016, MNRAS, 457, 4272, doi: 10.1093/mnras/stw183

Sesana, A., & Figueroa, D. G. 2025, arXiv e-prints, arXiv:2512.18822, doi: 10.48550/arXiv.2512.18822

Snyder, G. F., Lotz, J. M., Rodriguez-Gomez, V., et al. 2017, MNRAS, 468, 207, doi: 10.1093/mnras/stx487

Ventou, E., Contini, T., Bouché, N., et al. 2019, A&A, 631, A87, doi: 10.1051/0004-6361/201935597

Volonteri, M., Haardt, F., & Madau, P. 2003, ApJ, 582, 559, doi: 10.1086/344675

Xu, H., Chen, S., Guo, Y., et al. 2023, Research in Astronomy and Astrophysics, 23, 075024, doi: 10.1088/1674-4527/acdfa5

Zic, A., Reardon, D. J., Kapur, A., et al. 2023, Publications of the Astronomical Society of Australia, 40, doi: 10.1017/pasa.2023.36

Ringraziamenti

La statistica dice che se stai leggendo questo testo c'è una probabilità del 98.3% non hai nulla, ma proprio nulla da fare; molto probabilmente dovresti tornare a lavorare invece di perdere tempo leggendo questa paginetta. Se nonostante questo mio avvertimento sei ancora convinto di voler buttare del tempo leggendo i ringraziamenti di questa tesi, sei automaticamente mio fratello/sorella visto che sei un procrastinatore seriale. In ogni caso, ecco la lista delle persone da ringraziare: innanzitutto ringrazio i miei genitori, mio padre Bruno e mia madre Monica, le mie nonne Anna e Luciana e i parenti tutti che se non li ringrazio subito mi fanno una testa tanta (giustamente): che pacienza che avete avuto a sopportarmi da bambino! Vorrei ringraziare il gruppo di pelati di Pesaro Sam, Ciob, Alex, Luca e il più pelato di tutti, Brian, per la compagnia: meno male che l'alopecia non è contagiosa altrimenti sarei già pelato come voi. P.S. vi offro una bevuta allo Tzènghne. Vorrei ringraziare i capelluti di Bologna, Giò, Carlo, Fra, Louis, GP e GB, Ceci, Carla, il nostro super-papà preferito Riccà, e Morena, per tutte le risate e la compagnia che ci siamo fatti in questi anni di università: i migliori compagni di corso possibili. Vorrei anche ringraziare i pelati di Bologna, ciao Valè, grazie per l'alloggio all'ultimo anno, sei il top 1 coinquilino di sempre. Chiaramente vorrei anche ringraziare il Prof. Nipoti per la sua immensa pazienza e disponibilità in questi mesi di lavoro. Ultima ma non per importanza, vorrei ringraziare anche Alice, la mia diva preferita. Dai ma veramente c'è qualcuno che si sta leggendo questa smanfrina? Bello spreco di tempo vecchio/a, io rivaluterei le mie priorità fossi in te. Infine, se stai ancora leggendo e buttando il tuo tempo, ti sei guadagnato un premio, alla faccia di chi dice che procrastinare non paga: gli ultimi ringraziamenti sono per dell'ottima musica, quindi se proprio non hai nulla da fare ti consiglio di ascoltarla. Ringrazio tutti gli autori della musica nelle playlist "CHILL SUMMER VIBES", "Exquisit 90-00's Hip Hop", "2000s Complete Party" e "ブラ イアンはハゲの男だ" su Spotify. Infine vorrei che tu che stai leggendo ringraziassi me per averti fatto passare qualche minuto, ma solamente perchè ti voglio rispondere citando il buon Francesco Latorraca: "Ma no, grazie a te!".